Atmos. Chem. Phys., 15, 9435–9453, 2015
www.atmos-chem-phys.net/15/9435/2015/
doi:10.5194/acp-15-9435-2015

Atmospheric Chemistry and Physics
Open Access

Investigation of post-depositional processing of nitrate in East Antarctic snow: isotopic constraints on photolytic loss, re-oxidation, and source inputs

G. Shi[1,2], A. M. Buffen[2], M. G. Hastings[2], C. Li[3], H. Ma[1], Y. Li[1], B. Sun[1], C. An[1], and S. Jiang[1]

[1]Key Laboratory for Polar Science of State Oceanic Administration, Polar Research Institute of China, Shanghai 200062, China
[2]Department of Earth, Environmental and Planetary Sciences and Institute at Brown for Environment and Society, Brown University, Providence, Rhode Island 02912, USA
[3]The State Key Laboratory of the Cryospheric Sciences, Cold and Arid Regions Environmental and Engineering Research Institute, Chinese Academy of Sciences, Lanzhou 730000, China

Correspondence to: M. G. Hastings (meredith_hastings@brown.edu)

Received: 25 October 2014 – Published in Atmos. Chem. Phys. Discuss.: 18 December 2014
Revised: 16 July 2015 – Accepted: 16 July 2015 – Published: 24 August 2015

Abstract. Snowpits along a traverse from coastal East Antarctica to the summit of the ice sheet (Dome Argus) are used to investigate the post-depositional processing of nitrate (NO_3^-) in snow. Seven snowpits from sites with accumulation rates between 24 and 172 kg m^{-2} a^{-1} were sampled to depths of 150 to 300 cm. At sites from the continental interior (low accumulation, < 55 kg m^{-2} a^{-1}), nitrate mass fraction is generally > 200 ng g^{-1} in surface snow and decreases quickly with depth to < 50 ng g^{-1}. Considerably increasing values of δ^{15}N of nitrate are also observed (16–461 ‰ vs. air N_2), particularly in the top 20 cm, which is consistent with predicted fractionation constants for the photolysis of nitrate. The δ^{18}O of nitrate (17–84 ‰ vs. VSMOW (Vienna Standard Mean Ocean Water)), on the other hand, decreases with increasing δ^{15}N, suggestive of secondary formation of nitrate in situ (following photolysis) with a low δ^{18}O source. Previous studies have suggested that δ^{15}N and δ^{18}O of nitrate at deeper snow depths should be predictable based upon an exponential change derived near the surface. At deeper depths sampled in this study, however, the relationship between nitrate mass fraction and δ^{18}O changes, with increasing δ^{18}O of nitrate observed between 100 and 200 cm. Predicting the impact of post-depositional loss, and therefore changes in the isotopes with depth, is highly sensitive to the depth interval over which an exponential change is assumed. In the snowpits collected closer to the coast (accumulation > 91 kg m^{-2} a^{-1}), there are no obvious trends detected with depth and instead seasonality in nitrate mass fraction and isotopic composition is found. In comparison to the interior sites, the coastal pits are lower in δ^{15}N (−15–71 ‰ vs. air N_2) and higher in δ^{18}O of nitrate (53–111 ‰ vs. VSMOW). The relationships found amongst mass fraction, δ^{15}N, δ^{18}O and Δ^{17}O ($\Delta^{17}O = \delta^{17}O - 0.52 \times \delta^{18}O$) of nitrate cannot be explained by local post-depositional processes alone, and are instead interpreted in the context of a primary atmospheric signal. Consistent with other Antarctic observational and modeling studies, the isotopic results are suggestive of an important influence of stratospheric ozone chemistry on nitrate formation during the cold season and a mix of tropospheric sources and chemistry during the warm season. Overall, the findings in this study speak to the sensitivity of nitrate isotopic composition to post-depositional processing and highlight the strength of combined use of the nitrogen and oxygen isotopes for a mechanistic understanding of this processing.

1 Introduction

Nitrate (NO_3^-) is one of the major ions measured in Antarctic snow and ice. In the atmosphere, NO_3^- is formed by oxidation of NO and NO_2, which are collectively referred to as NO_x.

In the presence of sunlight, NO and NO_2 recycle rapidly with ozone (O_3), peroxy radical (HO_2), an organic radical (RO_2, where R = organics), or halogen radicals (XO, where X = Br, Cl or I) according to the following reactions:

$$NO + O_3 (\text{or } HO_2, RO_2, XO) \rightarrow NO_2 + O_2, \quad \text{(R1)}$$

$$NO_2 + O_2 \xrightarrow{h\nu} NO + O_3. \quad \text{(R2)}$$

During the day, i.e., when sunlight is present, oxidation of NO_2 by the hydroxyl radical (OH) produces nitric acid (HNO_3):

$$NO_2 + OH + M \rightarrow HNO_3 + M. \quad \text{(R3)}$$

At night and in colder environments, oxidation of NO_2 by O_3 is promoted and HNO_3 can be formed from hydrolysis of dinitrogen pentoxide (N_2O_5),

$$NO_2 + O_3 \rightarrow NO_3 + O_2\,, \quad \text{(R4)}$$

$$NO_3 + NO_2 + M \rightleftharpoons N_2O_{5(g)} + M, \quad \text{(R5)}$$

$$N_2O_{5(g)} + H_2O_{(l)} + \text{surface} \rightarrow 2HNO_{3(aq)}. \quad \text{(R6)}$$

or by abstraction of a hydrogen atom by the nitrate radical (NO_3) from dimethyl sulfide (DMS) or a hydrocarbon (HC),

$$NO_3 + \text{DMS or HC} \rightarrow HNO_3 + \text{products}. \quad \text{(R7)}$$

Important NO_x inputs to the troposphere include fossil fuel combustion, biomass burning, soil microbial activity, lightning, and injection from the stratosphere (Delmas et al., 1997; Lee et al., 1997). There has been interest in using ice core NO_3^- records to reconstruct past atmospheric NO_x sources, and atmospheric loading and variability in concentration over time. Increasing NO_3^- concentrations in Greenland ice core records have been linked to increasing anthropogenic emissions (fossil fuel and/or agricultural) since the Industrial Revolution (Mayewski and Legrand, 1990; Hastings et al., 2009). In contrast, such increases in NO_3^- have not been observed in Antarctica (Wolff, 1995; Wolff et al., 2012), suggesting that concentrations in snow are mainly controlled by natural sources.

The partitioning of NO_x inputs using ice core NO_3^- concentrations is difficult, however, since concentration alone cannot identify specific NO_x sources, and NO_3^- can be lost from snow by post-depositional processes such as photolysis and possibly volatilization as HNO_3 (Wolff, 1995; Röthlisberger et al., 2000; Frey et al., 2009). Measurements of nitrogen and oxygen stable isotope ratios in NO_3^- provide further constraints for past NO_x sources and oxidation chemistry (Alexander et al., 2004; Hastings et al., 2009; Hastings, 2010). In the atmosphere, the oxygen isotopes in NO_3^- reflect the oxidants involved in the production of NO_3^- (e.g., Reactions (R1)–(R7) above; Hastings et al., 2003; Michalski et al., 2003; Alexander et al., 2009), and the nitrogen isotopes can reflect NO_x sources and possible imprints of transport and chemistry (Hastings et al., 2003; Elliott et al., 2007; Savarino et al., 2007; Morin et al., 2008; Altieri et al., 2013). However, post-depositional processing in snow can modify the isotopic composition of NO_3^-. At Dome C in East Antarctica (where the snow accumulation rate is $< 35\,\text{kg}\,\text{m}^{-2}\,\text{a}^{-1}$, i.e., typically $< 10\,\text{cm snow}\,\text{a}^{-1}$), NO_3^- mass fractions decrease from hundreds of $\text{ng}\,\text{g}^{-1}$ in surface snow to tens of $\text{ng}\,\text{g}^{-1}$ at a depth of 10 cm, and this decrease corresponds to large changes in isotopic composition (Röthlisberger et al., 2000; Blunier et al., 2005; Frey et al., 2009; Erbland et al., 2013) such that this processing should be identifiable where it occurs. The influence of post-depositional alteration on NO_3^-, however, appears closely related to annual snow accumulation and at sites with higher accumulation rates, such as Summit, Greenland ($200\,\text{kg}\,\text{m}^{-2}\,\text{a}^{-1}$, i.e., 60 cm snow a^{-1}; Dibb and Fahnestock, 2004), the post-depositional effects are rather minor, and the atmospheric signal appears to be preserved (Hastings et al., 2004; Fibiger et al., 2013, and references therein).

In recent studies, the spatial variability of photolytic and volatile NO_3^- loss in East Antarctic upper snow has been investigated (Frey et al., 2009; Erbland et al., 2013), and represents important progress in understanding air–snow transfer of NO_3^-. However, there are still a number of questions regarding the interpretation of NO_3^- isotopes due to the complicated post-depositional behavior of NO_3^-. Distinguishing the form, extent and relative importance of the different possible isotope effects associated with post-depositional processes is critical for understanding what NO_3^- in an ice core represents.

In this study, samples from 150 to 300 cm deep snowpits, have been collected at seven sites along a traverse from the East Antarctic coast to Dome Argus (Dome A: the summit of the Antarctic ice sheet), and mass fraction and isotopic composition of NO_3^- were determined. The key objectives of this study are the following: (1) to investigate the effects of post-depositional processes on isotopic composition of NO_3^- at different depths in the snowpack; and (2) to understand the variation of NO_3^- isotopes in different environments across the East Antarctic Ice Sheet (EAIS). The results of this study are of significance to a further understanding of post-depositional processing of snow NO_3^- and the interpretation of NO_3^- isotopic composition archived in ice cores.

2 Materials and methods

2.1 Sample collection

The Chinese National Antarctic Research Expedition (CHINARE) team conducts an annual inland traverse from the coastal Zhongshan Station (Indian Ocean sector) to Dome A in East Antarctica (Fig. 1). This traverse covers a distance of about 1250 km. On the traverse route from Zhongshan to Dome A, seven snowpits were excavated during the 2012–2013 austral summer season (Fig. 1). Full information about each pit, including location, snow depth, sampling resolu-

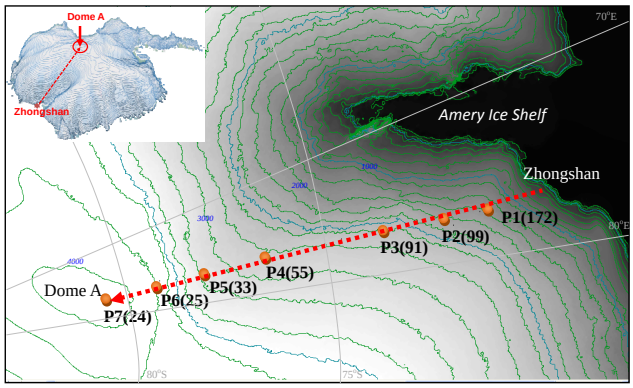

Figure 1. Snowpit locations sampled during the 2012–2013 Chinese National Antarctic Research Expedition (CHINARE) inland traverse. The numbers in parentheses denote the annual snow accumulation rates ($kg\,m^{-2}\,a^{-1}$) which are extended to 2013 from bamboo stick field measurements (Ding et al., 2011).

tion, collection date, mean annual snow accumulation, etc., is summarized in Table 1.

Snowpits were excavated manually and one snow wall was scraped clean and flat with a high-density polyethylene (HDPE) scraper. Snow samples were collected using 250 mL narrow-mouth HDPE vials pushed horizontally into the snow wall beginning at the bottom of the pit and moving upwards. The scraper and vials were pre-cleaned with Milli-Q ultrapure water (> 18.2 MΩ), dried in a class 100 super clean hood at 20 °C and then sealed in the clean polyethylene (PE) bags that were not opened until the field sampling started. Field blanks consisting of sampling bottles filled with Milli-Q water were analyzed for ion concentrations. All personnel wore PE gloves and face masks, and the pit sites were generally 1 km away from the traverse route to avoid possible contamination from expedition team activities. After collection, the vials were again sealed in clean PE bags and preserved in a clean insulated cabinet. All together, 530 snow samples were collected. All samples were transported to China in a freezer at −25 °C and then shipped frozen to Brown University in Providence, RI, USA.

2.2 Sample analysis

Snow NO_3^- mass fractions (denoted as $w(NO_3^-)$ in the following context) were determined using a Westco Scientific SmartChem 200 discrete chemistry analyzer. The standard deviation (SD) of $w(NO_3^-)$ of 55 field blanks run within sets of samples was $0.8\,ng\,g^{-1}$, which is comparable to blank Milli-Q water run on the same system. The pooled standard deviation of samples run in replicate ($n = 50$) in different sample sets is $1.5\,ng\,g^{-1}$.

Snow NO_3^- isotopic compositions were measured according to the denitrifier method by using denitrifying bacteria to convert NO_3^- to N_2O gas, which is collected and injected into a stable isotope ratio mass spectrometer (IRMS; Thermo Scientific DELTA V Plus; Sigman et al., 2001; Casciotti et al., 2002; Kaiser et al., 2007). At Brown, a minimum of 5 nmol of NO_3^- is required for an accurate isotopic determination of $^{15}N/^{14}N$ and $^{18}O/^{16}O$ ratios in snow samples with $w(NO_3^-)$ as low as $10.0\,ng\,g^{-1}$, which can be analyzed directly without a pre-concentration step (i.e., for a 5 nmol NO_3^- run, a sample of $10.0\,ng\,g^{-1}$ requires a 31 mL injection).

NO_3^- isotopic ratios ($\delta^{15}N(NO_3^-)$, $\delta^{17}O(NO_3^-)$, $\delta^{18}O(NO_3^-)$) are defined as

$$\delta = R_{sample}/R_{standard} - 1, \quad (1)$$

where R is the ratio of $n(^{15}N)/n(^{14}N)$, $n(^{17}O)/n(^{16}O)$, or $n(^{18}O)/n(^{16}O)$, with n representing the amount of substance. $\delta^{15}N(NO_3^-)$ and $\delta^{18}O(NO_3^-)$ values are reported in per mil (‰) relative to atmospheric N_2 ($\delta^{15}N_{air} = 0$ ‰) and Vienna Standard Mean Ocean Water ($\delta^{18}O_{VSMOW} = 0$ ‰), respectively. All of the $\delta^{15}N(NO_3^-)$ isotopic data were calibrated using the international reference materials IAEA-NO-3, USGS34 and USGS32, and $\delta^{18}O(NO_3^-)$ were calibrated using IAEA-NO-3, USGS34, and USGS35 (Michalski et al., 2002; Böhlke et al., 2003). Determining the isotopic composition in large volume samples has been extensively tested in the laboratory, and it is critical to run reference materials very close to the same concentrations (i.e., same volume injections) as samples, to eliminate any potential volume effects. Included in the supplementary materials are data from internal working standards that show excellent reproducibility over a variety of injection volumes in different runs (Tables S1 and S2 in the Supplement). Precision of the isotopic analyses is calculated in two ways (Buffen et al., 2014). First, the pooled standard deviation ($1\sigma_p$) of all standards run within individual sample sets was calculated. For $\delta^{15}N(NO_3^-)$, the $1\sigma_p$ of standards is 0.3 ‰ (IAEA-NO-3, $n = 80$), 0.3 ‰ (USGS34, $n = 80$), 1.1 ‰ (USGS32, $n = 53$) and 0.4 ‰ (USGS35, $n = 80$); and for $\delta^{18}O(NO_3^-)$ this is 0.6 ‰ (IAEA-NO-3, $n = 80$), 0.6 ‰ (USGS34, $n = 80$), 0.7 ‰ (USGS32, $n = 53$) and 0.7 ‰ (USGS35, $n = 80$). Second, the pooled standard deviation of all replicate samples run in at least two different sets was examined ($n = 38$ pairs of samples) and yielded 0.8 ‰ for $\delta^{15}N(NO_3^-)$ and 0.5 ‰ for $\delta^{18}O(NO_3^-)$. The pooled standard deviation of the replicate samples is probably the most representative measure of precision as it accounts for the total variation within the denitrifier method (i.e., from sample preparation to isotopic determination), and the variance is not diluted compared to the much higher number of standards that are pooled across sample sets (compared to individual samples that are only run once or twice).

During the NO_3^- reduction by bacteria, a small number of oxygen atoms may be exchanged between water and the intermediates of denitrification (e.g., NO_2^-) and must be corrected for the isotopic determination. In general, this exchange is < 10 %, and typically < 3 %, of the total O atoms

Table 1. Summary information for the seven snowpits presented in this study.

Snowpit	Location	Elevation m	Distance from coast, km	Mean annual accumulation, kg m^{-2} a^{-1} [a]	Mean annual temperature, °C [b]	Depth cm	Sampling resolution, cm	Sampling date, D.M.Y
P1	71.13° S, 77.31° E	2037	200	172.0	−29.12	150	3.0	18 Dec 2012
P2	71.81° S, 77.89° E	2295	283	99.4	−32.87	200	5.0	20 Dec 2012
P3	73.40° S, 77.00° E	2545	462	90.7	−35.72	200	5.0	22 Dec 2012
P4	76.29° S, 77.03° E	2843	787	54.8	−41.28	200	2.0	28 Dec 2012
P5	77.91° S, 77.13° E	3154	968	33.3	−46.37	200	2.0	30 Dec 2012
P6	79.02° S, 76.98° E	3738	1092	25.4	−53.13	200	2.5	2 Jan 2013
P7	80.42° S, 77.12° E	4093	1256	23.5	−58.50	300	2.5	6 Jan 2013

[a] Mean annual snow accumulation rates are obtained from bamboo stick field measurements, updated to 2013 from Ding et al. (2011). [b] Mean annual temperatures are derived from 10 m borehole temperatures and automatic weather station observations (Ding et al., 2010; Xiao et al., 2013).

in the produced N_2O and is corrected for using the measured oxygen isotope compositions of snow ($\delta^{18}O(H_2O)$) and water in the bacteria/media (see Casciotti et al., 2002; Kaiser et al., 2007 for correction schemes). $\delta^{18}O(H_2O)$ was determined using the standard CO_2 equilibration method (Johnsen et al., 1997). The standard deviation of reference (VSMOW) measurements ($n = 20$) was 0.10 ‰ . Full snowpit profiles of $\delta^{18}O(H_2O)$ were only completed for P1 and P7; only surface snow samples (3 cm) were measured for P2–P6.

A correction is also needed for $\delta^{15}N(NO_3^-)$ to account for the contribution of the $^{14}N^{14}N^{17}O$ isotopologue to the m/z 45 signal measured by the IRMS (Kaiser et al., 2007). Because atmospheric NO_3^- contains a non-zero $\Delta^{17}O$ (i.e., $\Delta^{17}O = \delta^{17}O – 0.52 \times \delta^{18}O > 0$ ‰), simply assuming $\delta^{17}O = 0.52 \times \delta^{18}O$ can yield an overestimate of the true $\delta^{15}N(NO_3^-)$ by as much as 1–2 ‰ (Sigman et al., 2001; Hastings et al., 2003). To account for this contribution, a measured or estimated $\Delta^{17}O(NO_3^-)$ is used to correct the $\delta^{15}N(NO_3^-)$ values. Previous East Antarctic investigations have shown that $\Delta^{17}O(NO_3^-)$ mainly ranges from 25 to 35 ‰ in snow NO_3^- (Erbland et al., 2013) and we find a similar range for P1 in our study (see below). For P1, the measured $\Delta^{17}O(NO_3^-)$ values reported below were used to correct $\delta^{15}N(NO_3^-)$, while a mid-range value of $\Delta^{17}O(NO_3^-) = 30$ ‰ was used for P2–P7. Using this mid-range value of $\Delta^{17}O(NO_3^-) = 30$ ‰ leads to an average $\delta^{15}N(NO_3^-)$ difference of 1.6 ‰ compared to using $\Delta^{17}O(NO_3^-) = 0$ ‰. A difference of ±5 ‰ in the $\Delta^{17}O(NO_3^-)$ used to correct the data (i.e., $\Delta^{17}O(NO_3^-) = 25$ or 35 ‰) results in a $\delta^{15}N(NO_3^-)$ difference of 0.3 ‰, which is comparable to our reported analytical precision and is negligible when compared to the range of sample $\delta^{15}N(NO_3^-)$ values.

For determination of $\Delta^{17}O(NO_3^-)$, the sample N_2O produced by the denitrifier method was thermally decomposed to N_2 and O_2 in a heated gold tube, and the O_2 was then measured at m/z 32 and 33 signals on the IRMS (Kaiser et al., 2007). A minimum of 35 nmol NO_3^- is needed for the analysis, but the low $w(NO_3^-)$ and low sample volumes available in this study limited the measurement of both $\Delta^{17}O(NO_3^-)$ and $\delta^{15}N$ and $\delta^{18}O$ on the same sample. A pre-concentration procedure is therefore needed for the measurement of $\Delta^{17}O(NO_3^-)$ (e.g., Morin et al., 2008; Frey et al., 2009; Erbland et al., 2013). Briefly, NO_3^- was trapped in an anion exchange resin, and then eluted by a 1M NaCl solution. A variety of NaCl salts (including the products of Fisher Scientific, Extrapure, and Macron) were tested and found to contain NO_3^-, and thus procedural blanks were determined for each batch of NaCl used. (Note that NO_3^- was found in every batch of NaCl tested, with values as high as 547 ng g^{-1} in the salt, and was different even for bottles with the same lot number.) For the samples from P1, 28 ng g^{-1} was measured for the 1M solution of NaCl (Fisher Scientific) used for elution. During the concentrating procedure, one Milli-Q water blank and two sets of standards (USGS34 and USGS35) with similar $w(NO_3^-)$ to the snow samples were processed simultaneously. The measured $\Delta^{17}O(NO_3^-)$ was then corrected by two steps: (1) $\Delta^{17}O(NO_3^-)$ in concentrated samples was linearly corrected using the standards USGS34 and USGS35 run within individual sample sets; and (2) the output of step (1) was further corrected by the standards used during the concentration procedure to account for the impact of procedural influence (e.g., the NaCl blank). A mean difference of 2.5 ‰ for $\Delta^{17}O(NO_3^-)$ was obtained between the results corrected by step (2) and data without the step (2) correction. Precision for repeated measurement of $\Delta^{17}O(NO_3^-)$ is only 0.44 ‰ (see also Table S2 in the Supplement), but without correcting for the blank associated with the eluent NaCl, we find that the pre-concentration method can result in an underestimation at least on the order of 2.5 ‰ for $\Delta^{17}O(NO_3^-)$.

3 Results

3.1 Snowpit $w(NO_3^-)$

A summary for all measurements of $w(NO_3^-)$, $\delta^{15}N(NO_3^-)$ and $\delta^{18}O(NO_3^-)$ in each snowpit is given in Fig. 2 and the detailed profiles with depth are illustrated in Fig. 3. In general, $w(NO_3^-)$ is lower than 200 ng g^{-1} in P1 and P2, which are characterized with higher annual snow accumulation (see Fig. 1), and large, quasi-regular fluctuations of $w(NO_3^-)$ are

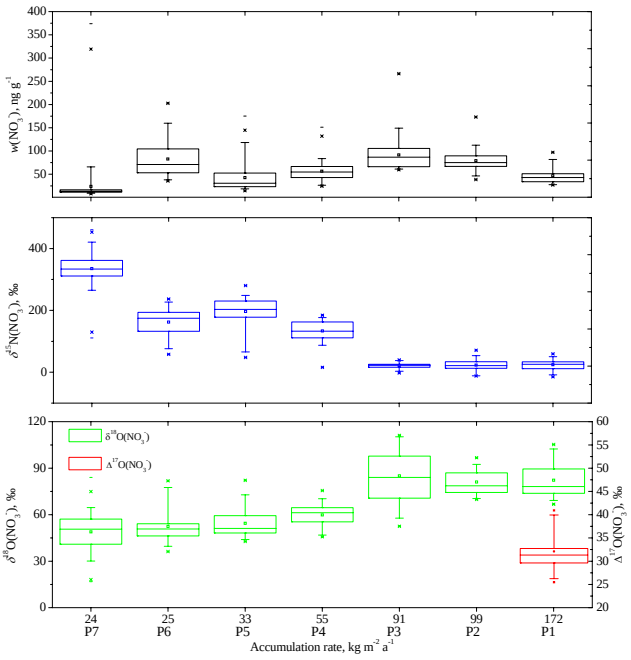

Figure 2. Statistics of mass fraction and isotopic compositions of NO_3^- for each snowpit (P1–P7), plotted as a function of snow accumulation rate. Box and whisker plots represent maximum (top end dash symbol for each box), minimum (bottom end dash symbol for each box), the range 1–99 % (top and bottom X symbol for each box), percentiles (5th, 25th, 75th, and 95th), and median (50th, solid line) and mean (open square near center of each box). Note that the data of $\Delta^{17}O(NO_3^-)$ are only available for P1 snowpit and refer to the right-hand axis.

present in both pits. In contrast, pits P4–P7 from the lower snow accumulation sites show the highest $w(NO_3^-)$ in surface snow, which falls sharply from $>200\,ng\,g^{-1}$ near the surface to below $50\,ng\,g^{-1}$ within the top meter, and do not contain regular fluctuations. The markedly decreasing trend of $w(NO_3^-)$ with depth seems to fit an exponential model as has been seen previously (Traversi et al., 2009).

3.2 Isotopic compositions of NO_3^-

For $\delta^{15}N(NO_3^-)$ and $\delta^{18}O(NO_3^-)$, the coastal and inland pits differ greatly in terms of the average values and the variability with depth. For the coastal sites P1–P3, $\delta^{15}N(NO_3^-)$ is generally lower than in the inland snowpits P4–P7, varying between −14.8 and 70.8 ‰, while $\delta^{15}N(NO_3^-)$ in the inland pits ranges from 15.5 to 460.8 ‰ (Figs. 2 and 3). This high value of 460.8 ‰ in pit P7 (which is at Dome A) is the highest natural $\delta^{15}N(NO_3^-)$ on Earth so far reported to our knowledge. In the inland pits (P4–P7), $\delta^{15}N(NO_3^-)$ is lower in the uppermost layers and strongly increases deeper in the snowpack, with most of the increase occurring in the top 20–30 cm.

In contrast to $\delta^{15}N(NO_3^-)$, $\delta^{18}O(NO_3^-)$ is higher on average in the coastal pits (P1–P3), ranging between 52.5 and 111.2 ‰, compared to the inland sites (P4–P7), where $\delta^{18}O(NO_3^-)$ varies between 16.8 and 84.0 ‰ (Figs. 2 and 3). It is noted that the averages of $\delta^{18}O(NO_3^-)$ for P4–P7 are comparable, while $\delta^{15}N(NO_3^-)$ means vary significantly, from 133.6 to 335.2 ‰. There is no obvious trend in the $\delta^{18}O(NO_3^-)$ profiles with depth in P1–P3, but this is not the case for the inland sites. $\delta^{18}O(NO_3^-)$ decreases over the top 20–30 cm, but gradual and consistent increases are observed below 30 cm in P4, P5 and P7 which continue to the pit base (200–300 cm; Fig. 3). A similar decrease in $\delta^{18}O(NO_3^-)$ is observed in the top of P6, but it is not clear if an increasing trend exists in the profile below.

$\Delta^{17}O(NO_3^-)$ of P1 varies from 25.2 to 42.9 ‰, with an average of 32.8 ‰ (Fig. 2). In general, the variation trend of $\Delta^{17}O(NO_3^-)$ is similar to that of $\delta^{18}O(NO_3^-)$ (Fig. 7), and a close relationship was observed between the two ($R^2 = 0.77$, $p < 0.01$).

The difference between the coastal and inland pits observed here is similar to that observed in the Erbland et al. (2013) study. A comparison between the two studies is presented in the Supplement as Fig. S1.

4 Discussion

After deposition, NO_3^- can be lost from snow by photolysis and volatilization as HNO_3 (sometimes referred to as evaporation or physical release in other studies), and the extent of loss via these post-depositional processes is expected to be accumulation dependent (Röthlisberger et al., 2002; Grannas et al., 2007). At lower accumulation sites, NO_3^- loss is relatively high, synchronous with a large degree of isotopic fractionation (Blunier et al., 2005; Frey et al., 2009; Erbland et al., 2013). In contrast, post-depositional alteration of snow NO_3^- in high accumulation regions can be minor, and seasonal and interannual cycles can be preserved in the snowpack (e.g., Wagenbach et al., 1994; Hastings et al., 2004).

Based on the site differences in annual snow accumulation rate and the profile trends of $w(NO_3^-)$, $\delta^{15}N(NO_3^-)$ and $\delta^{18}O(NO_3^-)$, the seven pits are divided into two groups within the following discussion: group I includes the coastal, medium-high accumulation sites P1–P3 ($>91\,kg\,m^{-2}\,a^{-1}$) and group II are the low-accumulation and further inland sites P4–P7 ($<55\,kg\,m^{-2}\,a^{-1}$). Below we consider what processes (and fractionation constants) can explain observations from the group I and group II snowpits, and whether it is possible to predict values at depth based on the loss processes near the surface.

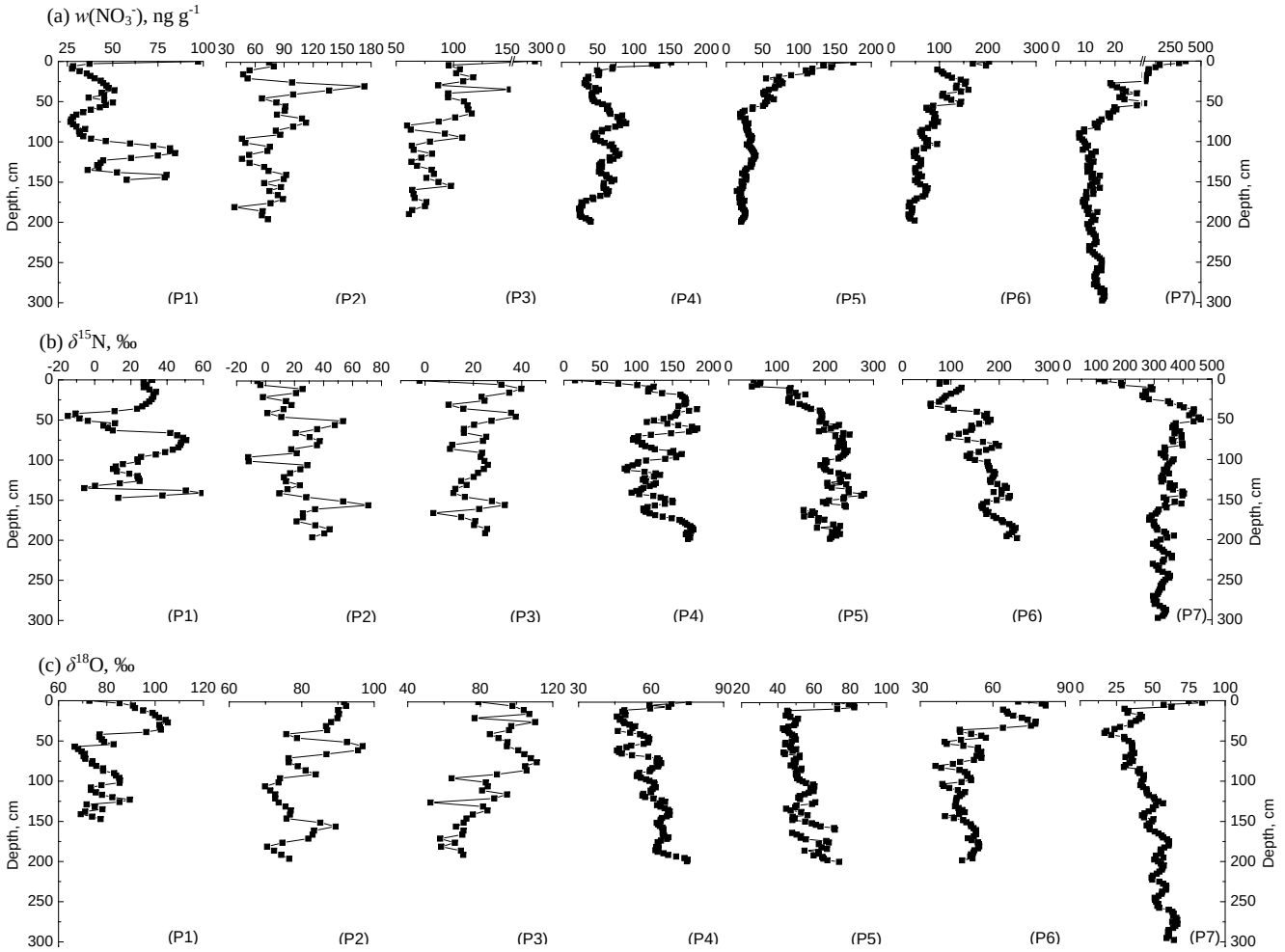

Figure 3. Detailed profiles of $w(NO_3^-)$ **(a)** and isotopic composition $\delta^{15}N$ **(b)** and $\delta^{18}O$ of NO_3^- **(c)** in the P1–P7 snowpits. Note that the x axis of $w(NO_3^-)$ in P3 and P7 was broken so the trend in the deeper snow can be seen.

4.1 NO_3^- loss in inland upper snowpack

If it is assumed that post-depositional loss of snow NO_3^- is accompanied by a Rayleigh-type fractionation, the observed changes in $\delta^{15}N$ and $\delta^{18}O$ in a snowpit profile can be described as a function of $w(NO_3^-)$ via

$$\ln(\delta_{snow}+1) = \varepsilon \times \ln(w_{snow}) + [\ln(\delta_{snow,0}+1) - \varepsilon \times \ln(w_{snow,0})], \quad (2)$$

where $\delta_{snow,0}$ and δ_{snow} denote isotopic ratios in the initial and remaining NO_3^-, respectively, and $w_{snow,0}$ and w_{snow} are the initial and remaining NO_3^- mass fractions, respectively (e.g., Blunier et al., 2005). ε can be obtained from the slope of the linear regression for $\ln(w_{snow})$ vs. $\ln(\delta_{snow}+1)$, while $[\ln(\delta_{snow,0}+1) - \varepsilon \times \ln(w_{snow,0})]$ would be the intercept. It is noted that ε is related to the fractionation factor α by $\varepsilon = \alpha - 1$ (Criss, 1999).

Solar radiation decreases exponentially in the snowpack, with attenuation described in terms of an e-folding depth (z_e) where the actinic flux is reduced to $1/e$ (37 %) of the surface value. Accordingly, roughly 95 % of snowpack photochemistry should occur above the depth of three times z_e (Warren et al., 2006). For the individual pits here, we calculate apparent ε values (ε_{app}) from data in the upper 20, 40 and 60 cm, to evaluate the impacts of post-depositional processes on snow NO_3^- (Table 2). Zatko et al. (2013) calculated a z_e of about 20 cm for remote Antarctic sites. For group II, relatively strong relationships are observed between $w(NO_3^-)$ and $\delta^{15}N(NO_3^-)$ or $\delta^{18}O(NO_3^-)$ in the top 60 cm (as indicated by the statistically significant R^2 values for Eq. (2); Table 2). These pits are characterized by negative $^{15}\varepsilon_{app}$, with values of −77.8 ‰ (P4), −93.1 ‰ (P5), −50.2 ‰ (P6) and −61.3 ‰ (P7) for the upper 20 cm snow layer (i.e., the 0–20 cm interval; Table 2); whereas $^{18}\varepsilon_{app}$ values are positive, indicating a depletion of $^{18}O(NO_3^-)$ with decreasing $w(NO_3^-)$. The observed fractionation constants ($^{15}\varepsilon_{app}$ and $^{18}\varepsilon_{app}$) for group II (P4–P7) are comparable to those from

other snowpits on the East Antarctic plateau (Frey et al., 2009; Erbland et al., 2013; see also Fig. S1 in the Supplement).

In the upper 20 cm of the snowpack, a significant NO_3^- loss with increasing depth is seen in the group II pits and corresponds to a large enrichment of $^{15}N(NO_3^-)$. A large loss of NO_3^- leading to such high $\delta^{15}N(NO_3^-)$ values in the surface snow is consistent with the calculated low $^{15}\varepsilon_{app}$ in the upper snowpack and our expectations based on other findings in East Antarctica (e.g., Savarino et al., 2007; Erbland et al., 2013). Such strongly positive $\delta^{15}N$ values (> 100 ‰) have not been observed in atmospheric NO_3^-.

4.1.1 Photolytic loss of NO_3^-

Photolysis of snow NO_3^- is thought to primarily occur within a disordered interface, sometimes referred to as a quasi-liquid layer, at the surface of the ice crystal via the reactions

$$NO_3^- + h\nu(+H^+) \rightarrow NO_{2(aq)} + OH \quad \text{(R8)}$$

$$NO_3^- + h\nu \rightarrow NO_2^- + O(^3P) \quad \text{(R9)}$$

$$NO_2^- + h\nu \rightarrow NO_{(aq)} + O^- \quad \text{(R10)}$$

$$NO_2^- + OH \rightarrow NO_{2(aq)} + OH^- \quad \text{(R11)}$$

with Reaction (R8) exceeding Reaction (R9) by a factor of 8–9 (Warneck and Wurzinger, 1988; Dubowski et al., 2001; Chu and Anastasio, 2003). Snow NO_3^- photolysis products are mainly NO_2, greatly exceeding NO under most conditions (Dibb et al., 2002). Under acidic conditions (pH < 5), $HONO_{(g)}$ formation from NO_2^- protonation is also important (Grannas et al., 2007 and references therein). Only NO_2 produced near the ice crystal surface–air interface can be released to the firn air and subsequently escape from the snowpack to the overlying atmosphere (Boxe et al., 2005).

In order to identify the relative importance of photolysis and volatilization (Sect. 4.1.3) on NO_3^- loss, the fractionation constant of each process should first be quantified. The photolysis rate constant $j_{NO_3^-}$ (s^{-1}) is expressed as

$$j_{NO_3^-} = \int \sigma_{NO_3^-}(\lambda, T)\phi_{NO_3^-}(\lambda, T, pH) I(\lambda) d\lambda, \quad (3)$$

where $\sigma_{NO_3^-}$ (cm^2) is the spectral absorption cross section; $\phi_{NO_3^-}$ is the quantum yield (0–1), and I is the spectral actinic flux (photons $cm^{-2}\,s^{-1}\,nm^{-1}$). Frey et al. (2009) proposed a theoretical model for estimating nitrate photolytic isotopic fractionation constants, which is based on a framework originally developed by Yung and Miller (1997) for stratospheric N_2O. The framework exploits mass-dependent differences in the vibrational frequencies and ground-state energies for a given set of isotopologues. These differences result in a modeled spectral absorption cross section for the heavier isotopologue which is shifted to longer wavelengths, thus influencing the rate constant. The isotopic fractionation constant can then be calculated by

$$\varepsilon = (j'/j) - 1, \quad (4)$$

where j' corresponds to the heavy isotopologue (e.g., $^{15}N^{16}O_3^-$); j corresponds to the light isotopologue (e.g., $^{14}N^{16}O_3^-$), and it is assumed that the different isotopologues retain similar spectral absorption curves and equal quantum yields.

We calculate the photolytic $^{15}\varepsilon$ and $^{18}\varepsilon$ at sites P1 and P7 for peak summer radiation conditions (solstice solar noon on 21 December 2012) using actinic fluxes derived from the Tropospheric Ultraviolet and Visible (TUV 5.0) radiation transfer model (Madronich and Flocke, 1998) assuming clear sky conditions and a total overhead ozone column of 300 DU for both sites. We use the nitrate absorption cross section from Chu and Anastasio (2003) and calculate quantum yields using the equation given in this same work for −10 °C at P1 ($\phi = 0.0040$) and −30 °C at P7 ($\phi = 0.0019$).

The resulting fractionation constants are $^{15}\varepsilon = -45.3$ ‰ (P1) to −48.0 ‰ (P7) and $^{18}\varepsilon = -32.5$ ‰ (P1) to −34.4 ‰ (P7), and the relatively small variability between the two sites indicates that the calculated values are representative for the two site groupings. Berhanu et al. (2014) have recently proposed absorption cross sections derived from the measurements of Chu and Anastasio (2003) but modeled directly for the $^{14}N^{16}O_3^-$ and $^{15}N^{16}O_3^-$ isotopologues at −30 °C. When using these cross sections, $^{15}\varepsilon$ is calculated to be −48.9 ‰ at P1 and −52.8 ‰ at P7.

The negative ε values suggest that photolysis will lead to a strong enrichment of both ^{15}N and ^{18}O in NO_3^- remaining in the snow. For $^{15}\varepsilon_{app}$ calculated from observations in the upper 60 cm of the group II pits (Table 2), the higher R^2 values imply that photolysis can largely explain enrichment of ^{15}N in NO_3^- with the decrease of $w(NO_3^-)$. At Dome C, where snow accumulation is typically less than 35 kg m^{-2} a^{-1}, close to the values of P4–P7 (Fig. 1), photolysis has also been reported as responsible for large increases in $\delta^{15}N(NO_3^-)$ with depth in the snow (Frey et al., 2009; Erbland et al., 2013). The negative calculated $^{18}\varepsilon$ (−32.5 to −34.4 ‰), however, does not agree with the highly positive $^{18}\varepsilon_{app}$ values based on the observations (Table 2).

4.1.2 Aqueous phase "secondary" NO_3^- formation

If the post-depositional loss of NO_3^- in the group II pits was driven solely by photolysis, ^{18}O should also be enriched in the remaining NO_3^- according to the modeled photolytic $^{18}\varepsilon$ values (−32.5 to −34.4 ‰). However, $\delta^{18}O$ decreases over the top 20 cm (Fig. 3) and the apparent $^{18}\varepsilon$ values ($^{18}\varepsilon_{app}$) calculated from the observed data in the upper 20 cm are instead positive, varying from 16.7 to 30.2 ‰ (Table 2). Furthermore, simple photolysis will lead to a linear relationship of $\delta^{18}O(NO_3^-)$ vs. $\delta^{15}N(NO_3^-)$ with a slope of roughly 0.7, i.e., equal to the ratio of the fractionation constants. How-

Table 2. Observed fractionation constants for ^{15}N and ^{18}O of NO_3^- ($^{15}\varepsilon_{app}$ and $^{18}\varepsilon_{app}$) calculated for different snow layer depths from the linear regression of $\ln(\delta_{snow}+1)$ vs. $\ln(w_{snow})$ in Eq. (2). Five different depth intervals were selected for calculating ε_{app}: 0–20, 0–40, 0–60 cm, 100 cm-bottom and the entire pit. Also given are the standard error (1σ), R^2 values and the significance level, p, where bolded values represent $p < 0.05$.

Snowpit	Depth	^{15}N			^{18}O		
		$^{15}\varepsilon_{app} \pm 1\sigma$, ‰	p	R^2	$^{18}\varepsilon_{app} \pm 1\sigma$, ‰	p	R^2
P1	0–20 cm	2.4 ± 2.0	0.379	0.157	**-15.3 ± 6.0**	**0.044**	**0.588**
	0–40 cm	-0.4 ± 5.0	0.943	0.000	-8.7 ± 7.0	0.248	0.109
	0–60 cm	-3.9 ± 14.0	0.785	0.004	-9.4 ± 10.0	0.368	0.043
	100-Bottom	17.2 ± 14.0	0.248	0.094	-6.5 ± 5.0	0.175	0.127
	Entire	-11.8 ± 7.0	0.098	0.056	-3.7 ± 4.0	0.390	0.015
P2	0–20 cm	-45.5 ± 26.0	0.184	0.497	**4.0 ± 1.0**	**0.017**	**0.887**
	0–40 cm	0.8 ± 10.0	0.936	0.001	-4.2 ± 4.0	0.274	0.167
	0–60 cm	4.1 ± 15.0	0.789	0.007	-2.1 ± 4.0	0.647	0.020
	100-Bottom	21.5 ± 16.0	0.197	0.091	**11.2 ± 4.2**	**0.015**	**0.287**
	Entire	11.9 ± 9.1	0.198	0.043	7.0 ± 3.6	0.060	0.090
P3	**0–20 cm**	**-36.8 ± 6.7**	**0.012**	**0.909**	-19.8 ± 13.5	0.237	0.420
	0–40 cm	**-27.5 ± 11.0**	**0.036**	**0.488**	-15.4 ± 11.0	0.188	0.233
	0–60 cm	**-28.8 ± 9.1**	**0.009**	**0.476**	-14.0 ± 8.7	0.135	0.192
	100-Bottom	12.3 ± 12.0	0.318	0.059	13.5 ± 18.6	0.478	0.030
	Entire	-1.2 ± 4.9	0.811	0.002	15.4 ± 8.0	0.061	0.092
P4	**0–20 cm**	**-77.8 ± 9.2**	**0.000**	**0.888**	**17.1 ± 3.1**	**0.000**	**0.778**
	0–40 cm	**-81.6 ± 7.5**	**0.000**	**0.868**	**14.0 ± 2.1**	**0.000**	**0.706**
	0–60 cm	**-73.3 ± 9.8**	**0.000**	**0.665**	**11.4 ± 2.5**	**0.000**	**0.419**
	100-Bottom	**-56.0 ± 5.3**	**0.000**	**0.703**	**-3.4 ± 1.3**	**0.011**	**0.126**
	Entire	**-58.7 ± 5.0**	**0.000**	**0.584**	1.4 ± 1.8	0.433	0.006
P5	**0–20 cm**	**-93.1 ± 23.6**	**0.003**	**0.633**	**30.2 ± 12.3**	**0.036**	**0.401**
	0–40 cm	**-92.1 ± 10.8**	**0.000**	**0.791**	**24.9 ± 5.5**	**0.000**	**0.522**
	0–60 cm	**-92.5 ± 8.1**	**0.000**	**0.820**	**16.0 ± 3.6**	**0.000**	**0.412**
	100-Bottom	27.3 ± 13.7	0.053	0.083	**-9.6 ± 4.0**	**0.022**	**0.114**
	Entire	**-56.9 ± 5.0**	**0.000**	**0.577**	0.0 ± 1.6	0.985	0.000
P6	**0–20 cm**	**-50.2 ± 7.3**	**0.000**	**0.880**	**16.7 ± 5.1**	**0.017**	**0.638**
	0–40 cm	**-63.0 ± 21.0**	**0.010**	**0.390**	16.2 ± 12.1	0.201	0.114
	0–60 cm	**-70.8 ± 25.1**	**0.010**	**0.265**	17.9 ± 9.3	0.066	0.145
	100-Bottom	**-61.3 ± 8.0**	**0.000**	**0.605**	**-7.8 ± 2.4**	**0.003**	**0.216**
	Entire	**-76.8 ± 5.8**	**0.000**	**0.694**	**11.3 ± 2.1**	**0.000**	**0.265**
P7	**0–20 cm**	**-61.3 ± 9.8**	**0.000**	**0.848**	**18.4 ± 4.1**	**0.003**	**0.738**
	0–40 cm	**-73.9 ± 8.5**	**0.000**	**0.834**	**16.4 ± 2.4**	**0.000**	**0.753**
	0–60 cm	**-81.0 ± 8.7**	**0.000**	**0.789**	**15.2 ± 1.9**	**0.000**	**0.728**
	100-Bottom	20.7 ± 14.4	0.154	0.026	10.0 ± 4.5	0.051	0.060
	Entire	**-31.5 ± 5.0**	**0.000**	**0.251**	-0.7 ± 1.7	0.690	0.001

ever, there are negative relationships between $\delta^{18}O(NO_3^-)$ and $\delta^{15}N(NO_3^-)$ in the top 20 cm (Fig. 4), with slopes varying from -0.4 to -0.2.

Similar negative relationships have been observed in other East Antarctic snowpits (Frey et al., 2009; Erbland et al., 2013) and, following from experimental and theoretical work (McCabe et al., 2005; Jacobi and Hilker, 2007), were attributed to the aqueous-phase re-oxidation of the products of NO_3^- photolysis (e.g., NO_2) by OH and/or H_2O to form "secondary" NO_3^-.

In this way, the O atoms from OH / H_2O provide a depleted ^{18}O source while $\delta^{15}N(NO_3^-)$ is seemingly not affected. For the group II pits, $\delta^{18}O(H_2O)$ in surface snow falls roughly in the range of -45 to -60 ‰. These effects can explain the observed positive $^{18}\varepsilon_{app}$ values and negative relationships between $\delta^{18}O(NO_3^-)$ and $\delta^{15}N(NO_3^-)$ in the top 20 cm. (Direct exchange of O atoms between NO_3^- and H_2O is only

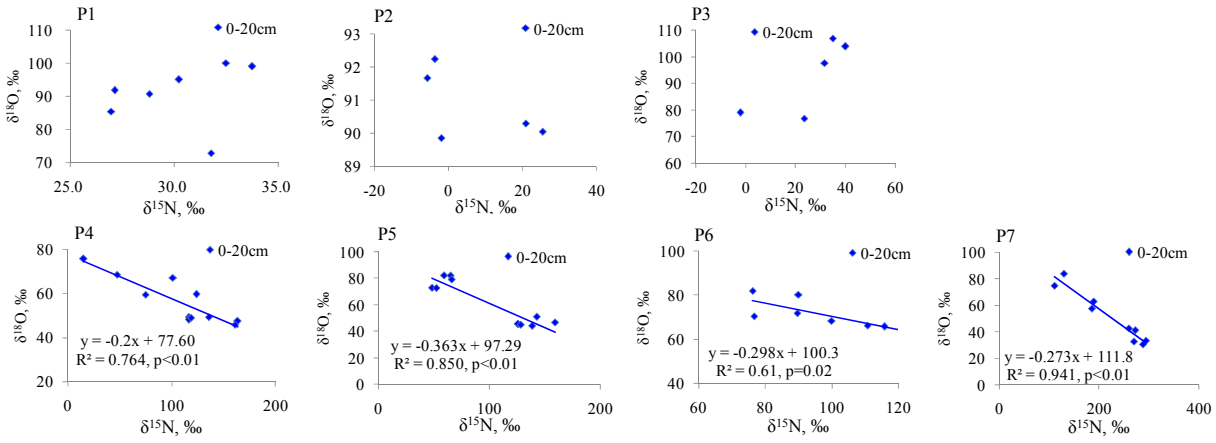

Figure 4. Relationships between δ^{18}O and δ^{15}N of NO_3^- in the topmost 20 cm of the snowpits. Least squares regressions are noted with lines and are significant at $p < 0.05$.

thought to be important at NO_3^- concentrations that are orders of magnitude higher than those found in snow (Bunton et al., 1952).)

For the top 2.5 cm of snow in P7, $w(NO_3^-)$ and $\delta^{18}O(NO_3^-)$ is 374 ng g^{-1} and 74.9 ‰ respectively, while $w(NO_3^-)$ decreases to 37.6 ng g^{-1} at a depth of 20 cm. Based on the modeled effect of photolysis, δ^{18}O in the remaining NO_3^- at 20 cm could be predicted by

$$\delta^{18}O_{remaining} = (1 + \delta^{18}O_0) f^{(^{18}\varepsilon)} - 1, \quad (5)$$

where $\delta^{18}O_{remaining}$ represents δ^{18}O in the remaining NO_3^-; $\delta^{18}O_0$ is that of initial NO_3^-; f is the fraction of NO_3^- remaining in the snow; and $^{18}\varepsilon$ is the photolysis fractionation constant (−34.4 ‰). If photolysis alone is responsible for the NO_3^- loss, $\delta^{18}O(NO_3^-)$ is expected to be 163 ‰ at 20 cm. Instead, at a depth of 20 cm the observed $\delta^{18}O(NO_3^-)$ is 42.6 ‰. This then would require a cumulative 54 % of the O atoms in the remaining NO_3^- to reflect that of water, assuming a $\delta^{18}O(H_2O)$ of −60 ‰. This back-of-the-envelope calculation would produce varying degrees of exchange amongst the inland snowpits (group II) due to the difference in mass fraction and $\delta^{15}N(NO_3^-)$ and $\delta^{18}O(H_2O)$ in the upper snowpack. For this calculation to be more accurate the initial deposition of primary NO_3^- from the atmosphere should be known (vs. that remaining in the surface snow sample collected for study) and it should be considered that the photolytic loss of NO_3^- and formation of secondary NO_3^- effectively happen simultaneously. Still, this simplified mass balance approach, overall, indicates that re-oxidation plays a significant role in determining how the δ^{18}O of NO_3^- evolves in the snow column during burial.

4.1.3 Volatile loss of NO_3^-

Volatilization, or physical release, of HNO_3 may also be a pathway for post-depositional loss of NO_3^- in snow (Röthlisberger et al., 2000; Erbland et al., 2013). The importance of this process is unclear, however, as loss proceeds only as HNO_3,

$$H^+_{(aq)} + NO_{3^-_{(aq)}} \rightleftharpoons HNO_{3(aq)} \rightleftharpoons HNO_{3(g)}, \quad (R12)$$

and thus requires highly acidic conditions given the very high dissociation constant for HNO_3 (Sato et al., 2008). Volatilization may also be inhibited at low temperatures as suggested by laboratory and field observations (Erbland et al., 2013; Berhanu et al., 2014).

The current understanding of the isotopic impact of volatilization is somewhat limited. An experiment conducted by Erbland et al. (2013) at Dome C suggested that the $^{15}\varepsilon$ (mean $\pm 1\sigma$) for volatilization varied from 0.9 ± 3.5 ‰ (−30 °C) to -3.6 ± 1.1 ‰ (−10 °C) (i.e., close to non-fractionating). However, the loss of NO_3^- in these experiments may have been driven by the large losses of snow via sublimation. No observational or experimental data for $^{18}\varepsilon$ are available. Theoretical model estimates of volatile fractionation, assuming that the aqueous-phase equilibrium in Reaction (R12) is the controlling step in the overall fractionation (Frey et al., 2009), predict values of $^{15}\varepsilon$ and $^{18}\varepsilon$ to be from 12.6 ‰ (0 °C) to 16.8 ‰ (−73 °C) and between 1.1 ‰ (0 °C) and 0.6 ‰ (−73 °C), respectively (Table S3 in the Supplement).

For the summertime temperatures at the P4–P7 sites (< −30 °C), physical release should deplete both ^{15}N and ^{18}O in the remaining snow NO_3^- according to the modeled ε values, whereas the field experiment observations would suggest negligible change in δ^{15}N with decreasing $w(NO_3^-)$ in the snow. The observations for P4–P7 show increasing $\delta^{15}N(NO_3^-)$ with decreasing $w(NO_3^-)$, and that $\delta^{15}N(NO_3^-)$

is negatively correlated with $\delta^{18}O(NO_3^-)$ (Fig. 4), disagreeing with both expectations (i.e., field experiment observations and modeled results; Table S3 in the Supplement). The current understanding of volatile fractionation, however, is very limited and experimental data for $^{18}\varepsilon$ are not available to date. This makes it hard to attribute the relationships between $w(NO_3^-)$ and $\delta^{15}N(NO_3^-)$ and $\delta^{18}O(NO_3^-)$ to volatilization at our sites given the existing state of knowledge.

4.2 Isotopic variability with depth at inland sites (group II snowpits)

As shown in Table 2, the logarithmic relationships between $\delta^{15}N$ or $\delta^{18}O$ and mass fraction of NO_3^- are strongest in the upper 60 cm of group II snowpits, as seen in the R^2 values. While generally weaker in the layers below, the R^2 values remain significant even when the entire snowpit is considered. For instance, for $^{15}\varepsilon_{app}$, P4, P5, and P6 all have R^2 above 0.5 (with a $p < 0.05$) when observations from the entire snowpit are considered. Interestingly, while $\delta^{15}N(NO_3^-)$ maintains a negative relationship with $w(NO_3^-)$ at all depths, the sign of apparent fractionation constant for $\delta^{18}O(NO_3^-)$ changed (Table 2; Fig. 5); i.e., the relationships between $\delta^{18}O(NO_3^-)$ and $w(NO_3^-)$ shift from being positive in the upper 20 cm to generally negative in the deeper snow (Fig. S2 in the Supplement). This leads to there generally being no association between $w(NO_3^-)$ and $\delta^{18}O(NO_3^-)$ when the entire snowpit depth interval is considered (Table 2).

It is also useful to discuss this variability with depth in terms of the isotopic fractionation constants. If there was only a single isotopically fractionating process driving the observed changes in the snow, such as photolysis, the apparent fractionation constants for $\delta^{15}N(NO_3^-)$ and $\delta^{18}O(NO_3^-)$ would be similar throughout the snow column. This expectation relies on two important assumptions. First, the boundary conditions that influence the fractionation constants remain similar over time. This is to say that factors such as the contribution of different NO_3^- sources, accumulation rate, the influence of total overhead ozone on the spectral actinic flux and photolysis rate, and the influence of snow chemistry on the photolability of NO_3^- (e.g., Davis et al., 2008; Meusinger et al., 2014), remain similar over time. Second, the isotopic imprint of photolysis is set in the upper snowpack and then preserved below. This requires the assumption that once NO_3^- is moved below the photic zone, no additional in situ modifications take place. Stemming from these expectations, the isotopic composition of buried NO_3^- could be back-calculated to that originally at the surface if the isotopic imprint of alteration at the surface could be quantified in terms of a fractionation constant.

Based on the observations with depth, it is clear that the ε_{app} values are dependent on the depth range chosen (Table 2). Both $^{15}\varepsilon_{app}$ and $^{18}\varepsilon_{app}$ vary but with distinct differences. The $^{15}\varepsilon_{app}$ tends to become more positive with depth, while $^{18}\varepsilon_{app}$ decreases and even switches from positive to negative values. When taken together with variability in the strength of the isotopic relationships with $w(NO_3^-)$ and the observation that isotopic composition continues to change below the expected photic zone depths, especially for $\delta^{18}O(NO_3^-)$ (Fig. 3), it would seem that the assumptions above do not all apply. Either the fractionation constants change over time because of a change in boundary conditions and/or the isotopic imprint of photolysis is not preserved below the photic zone. The former hypothesis is much more likely as, thus far, there is little other evidence of processes well below the photic zone modifying buried NO_3^-.

4.3 Predicting $w(NO_3^-)$, $\delta^{15}N(NO_3^-)$ and $\delta^{18}O(NO_3^-)$ values in buried snow

Erbland et al. (2013) proposed that snow $w(NO_3^-)$ and isotopic compositions may approach constant values, called "asymptotic" values, below the photic zone (or zone of active NO_3^- loss). By means of an exponential regression, asymptotic values are calculated by

$$M(x) = M_{(as.)} + [M_{(0)} - M_{(as.)}]e^{(-cx)}, \quad (6)$$

where $M_{(x)}$ is the $w(NO_3^-)$, $\delta^{15}N(NO_3^-)$ or $\delta^{18}O(NO_3^-)$ at depth x (cm); $M_{(as.)}$ is the asymptotic value for these parameters; $M_{(0)}$ is the value at the surface of the snowpit; and c is a constant. Asymptotic values for each snowpit are calculated from the best fit (minimizing the sum of squared residuals) of $M_{(x)}$ vs. depth.

Based on observations from only the top 20 cm of snow in different snowpits on the EAIS, the Erbland et al. (2013) study predicted values below the photic zone. Because our snowpits extend deeper along the entire traverse, and as seen in Fig. 3 the snowpits did not typically follow a simple exponential decrease, we explored whether the asymptotic values change when derived from different depth ranges in the snowpit. In order to compare the asymptotic values derived from different snow depth ranges, observations from four intervals (0–20, 0–40, 0–60, and 0–100 cm) were selected to make this calculation, and the results are listed in Table 3. Several interesting results emerge. For asymptotic calculations of $w(NO_3^-)$, $\delta^{15}N(NO_3^-)$ and $\delta^{18}O(NO_3^-)$, all show important variations depending on the depth interval over which they are calculated. The variance, described in Table 3 by the standard error, is relatively large for the asymptotic values, but generally decreases the more observations that are included. In concert with this, the greater amount of observations included in the calculation the better the fit of the predicted values with the observed values as evidenced by the changing R^2 with calculations over different depth intervals. The sensitivity of the calculation of asymptotic values for different depth intervals in each of the group II snowpits is shown in Fig. 6.

What is the depth interval over which it is necessary to calibrate the asymptotic calculation? In other words, how much

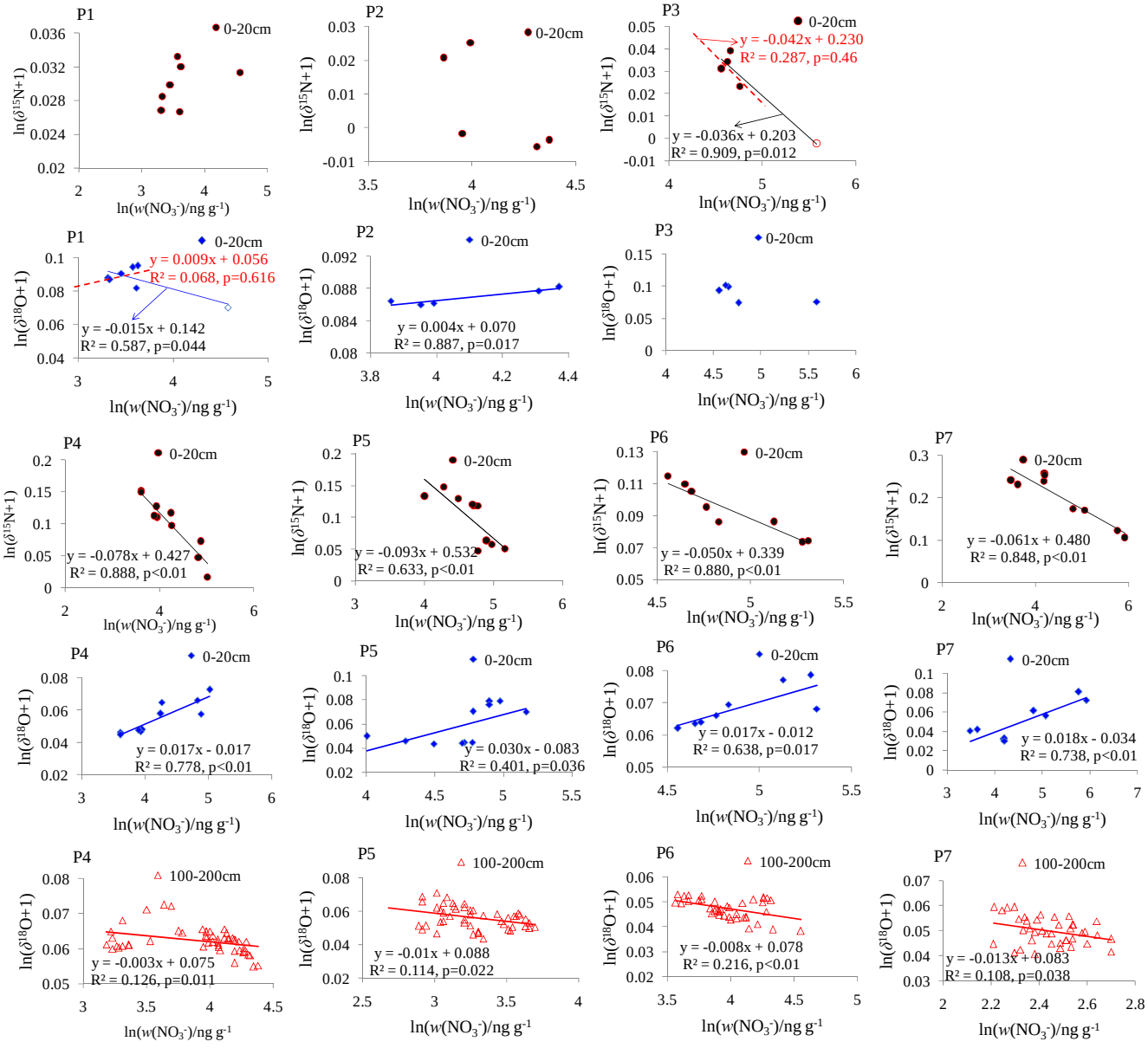

Figure 5. The relationships between $w(NO_3^-)$ and $\delta^{18}O$ and $\delta^{15}N$ of NO_3^- in the near surface (< 20 cm) and at depth (100–200 cm for group II snowpits) snow ranges. Least squares regressions are noted with lines and are significant at $p < 0.05$. It is noted that the linear regression slope for individual snowpits is the apparent fractionation constant ($^{15}\varepsilon_{app}$ and $^{18}\varepsilon_{app}$; Table 2). The red dashed lines in the panels of P3 ($\ln(\delta^{15}N + 1)$ vs. $\ln(w(NO_3^-))$) and P1 ($\ln(\delta^{18}O + 1)$ vs. $\ln(w(NO_3^-))$) are indicative of the change in the linear fit if the top most samples (open circle in P3, top row; open diamond in P1, second row) are removed.

information must we know about surface conditions to make the asymptotic relationship useful for predicting isotope values at depth? Figure 6 clearly shows that the more observations that are included the better the fit to the data will be, which is logical. But the range of profiles predicted by the asymptotic regressions also make it clear that much more information exists in the observations than can be explained by the simple assumption that photolytic loss, particularly in the top 20 cm, is the overwhelming signal captured at these low-accumulation sites. Overall, the $\delta^{18}O(NO_3^-)$ in deeper snow is more difficult to predict compared to $w(NO_3^-)$ and $\delta^{15}N(NO_3^-)$. This conclusion is consistent with the changes in $\delta^{18}O(NO_3^-)$ at deeper depths (Fig. 3) and the changes in ε_{app} with depth (Table 2).

In cases where there is significant post-depositional loss and/or processing of NO_3^-, the $\delta_{(as.)}$, in theory, could help account for the impact of post-depositional processing compared to preservation in reconstructing a primary

Table 3. Asymptotic values of $w(NO_3^-)$, $\delta^{15}N$ and $\delta^{18}O$ of NO_3^- calculated based on four different snow depth intervals (0–20, 0–40, 0–60 and 0–100 cm) of each snowpit. p is the significance level of observed data fitted using the exponential regression Eq. (6), and R^2 denotes the squared correlation coefficient of observed data compared to the regression model predicted values. Also given is the standard error (1σ) of asymptotic values.

Snowpit	Depth	$w(NO_3^-)_{(as.)}$, ng g^{-1}			$\delta^{15}N_{(as.)}$, ‰			$\delta^{18}O_{(as.)}$, ‰		
		$w(NO_3^-) \pm 1\sigma$	p	R^2	$\delta^{15}N \pm 1\sigma$	p	R^2	$\delta^{18}O \pm 1\sigma$	p	R^2
P4	0–20 cm	26.9 ± 15.7	0.00	0.92	165.4 ± 18.3	0.00	0.94	41.2 ± 7.4	0.00	0.88
	0–40 cm	38.1 ± 3.5	0.00	0.92	173.2 ± 5.4	0.00	0.95	49.2 ± 1.3	0.00	0.80
	0–60 cm	45.3 ± 2.7	0.00	0.83	158.4 ± 4.3	0.00	0.82	51.6 ± 1.1	0.00	0.58
	0–100 cm	54.5 ± 2.5	0.00	0.58	144.3 ± 3.9	0.00	0.51	54.5 ± 0.9	0.00	0.29
P5	0–20 cm	50.0 ± 4.3	0.00	0.82	166.2 ± 6.5	0.00	0.74	41.6 ± 3.1	0.00	0.63
	0–40 cm	39.6 ± 13.5	0.00	0.91	216.6 ± 58.7	0.00	0.95	43.5 ± 4.1	0.00	0.80
	0–60 cm	39.9 ± 6.1	0.00	0.92	277.9 ± 51.2	0.00	0.89	46.0 ± 1.8	0.00	0.71
	0–100 cm	25.8 ± 3.3	0.00	0.93	254.6 ± 10.6	0.00	0.92	48.2 ± 1.0	0.00	0.65
P6	0–20 cm	101.3 ± 32.9	0.00	0.73	106.4 ± 11.1	0.09	0.43	63.4 ± 38.4	0.20	0.26
	0–40 cm	131.1 ± 7.7	0.01	0.45	95.2 ± 7.4	0.45	0.04	48.3 ± 105.6	0.03	0.29
	0–60 cm	121.4 ± 6.7	0.00	0.39	160.1 ± 196.8	0.00	0.42	22.7 ± 15.0	0.00	0.54
	0–100 cm	40.4 ± 3.6	0.00	0.65	179.7 ± 54.5	0.00	0.43	39.9 ± 7.4	0.00	0.61
P7	0–20 cm	15.7 ± 26.9	0.00	0.96	298.7 ± 40.5	0.00	0.85	29.2 ± 18.5	0.00	0.73
	0–40 cm	22.3 ± 6.9	0.00	0.97	490.0 ± 23.0	0.00	0.90	23.2 ± 7.0	0.00	0.78
	0–60 cm	23.3 ± 3.9	0.00	0.97	448.7 ± 33.1	0.00	0.86	29.7 ± 2.5	0.00	0.75
	0–100 cm	17.9 ± 2.3	0.00	0.97	383.8 ± 9.4	0.00	0.75	33.9 ± 1.4	0.00	0.64

atmospheric signal. Our results show that $\delta_{(as.)}$ (and ε_{app}) is sensitive to the depth interval over which exponential change is assumed. As suggested above, changes in factors such as the contribution of different NO_3^- sources, accumulation rate, total overhead ozone, and the influence of snow chemistry on photolability of NO_3^- may not remain similar over the time period covered by the snowpits. There do not appear to be significant trends in the annual accumulation rates based on data from Dome A. Wang et al. (2013) have compiled existing stake and snowpit accumulation measurements from Dome A and show (1) little spatial variability (surrounding 50 km) and (2) stable accumulation rates over recent decades and since 1260 AD (1965–2009 = 21 kg m^{-2} a^{-1}; 2005–2008 = 18 kg m^{-2} a^{-1}; 2005–2009 = 19 kg m^{-2} a^{-1}; 2008–2009 = 21 kg m^{-2} a^{-1}; and 1260–2005 = 21.6 to 23 kg m^{-2} a^{-1}). Automatic weather station measurements presented in the same work show somewhat higher accumulation in the spring and summer (roughly 6–7 mm per month) vs. fall and winter (roughly 3–6 mm per month) with fairly stable values in the warmer months. Based on the Dome A studies, it is unlikely that significant changes in accumulation have occurred in the area of the group II snowpits. Therefore, this cannot explain the difference between what is predicted based upon the $\delta_{(as.)}$ and what is observed (Fig. 6). Nor does it seem likely that changes in ε_{app} can be explained by accumulation rate. If it is assumed that snow accumulation has been constant for the group II snowpits, then the snowpits can be roughly dated based on measured accumulation and snow density (Fig. S3). This approximate dating suggests that the bottom of the P4 snowpit is from about the year 2000; P5 dates from ∼1994; P6 from 1985; and P7 from 1970. All four snowpits show a change in the relationship between $\delta^{18}O(NO_3^-)$ with $w(NO_3^-)$ and with $\delta^{15}N(NO_3^-)$ between near surface snow (< 20 cm) and deeper snow (Fig. 5). Based on the approximate dating, the timing of this change is very different in the different snowpits. For example, for a depth of 100 cm, snow in P4 is dated to ∼2007, P5 to ∼2004, and P6 and P7 to ∼2000. (Even given the imprecision of the dating method it is unlikely that more accurate dating would conclude that changes in the snowpits occur exactly together.)

Can changes in stratospheric ozone concentration help to explain this change? Both the photolytic rate constant and fractionation constants would be sensitive to significant changes in overhead ozone concentration (i.e., less stratospheric ozone leads to more penetration of light at wavelengths that can photolyze NO_3^-). Based on the approximate dating of the pits, P7 overlaps with the pre-ozone hole era (generally considered prior to 1980), but there is no obvious change in the isotope observations (1980 occurs at a depth of about 250 cm; Figs. 3 and S3). Moreover, both ground-based observations at the South Pole and satellite-based observations (TOMS/OMI) do not show any significant trend in total overhead ozone during spring and early summer over the time period 2000–2010

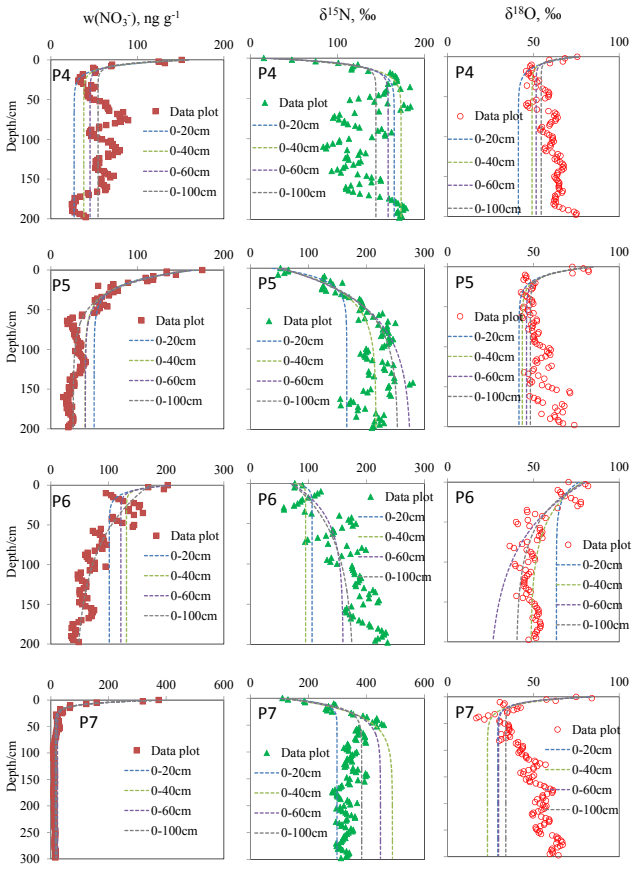

Figure 6. Detailed profiles of $w(NO_3^-)$, $\delta^{15}N$ and $\delta^{18}O$ of NO_3^- in different snow depth intervals (0–20, 0–40, 0–60, and 0–100 cm) for the snowpits P4-P7. The dashed lines are the best fit regressions for the observed data, and asymptotic values are calculated for $w(NO_3^-)$, $\delta^{15}N$ and $\delta^{18}O$ of NO_3^- by Eq. (6).

(http://www.antarctica.ac.uk/met/jds/ozone/graphs.html; http://www.cpc.noaa.gov/products/stratosphere/winter_bulletins/sh_09/; http://ozonewatch.gsfc.nasa.gov/statistics/annual_data.html). This does not prove that there is not a link between the observed changes in the isotopic composition of snow NO_3^- and overhead ozone concentration, but this link over time is not obvious in this region. Finally, it is notable that the DC07 and DC04 pits (about 70 cm) from Frey et al. (2009) cover 8–10 years and thus overlap some with data from P4–P7. Neither of the DC pits show increasing $\delta^{18}O(NO_3^-)$ with depth (or decreasing $\delta^{15}N(NO_3^-)$ such as that in P7). Given the large spatial influence of stratospheric ozone on surface irradiance in Antarctica, it seems unlikely that Dome A and its surrounding region would be affected by this process and not Dome C. This suggests that something more localized, such as a change in the photolability of NO_3^- due to changes in snow chemistry, may have an important influence in recent decades.

4.4 Seasonal shifts in NO_3^- sources to coastal snow (group I snowpits)

Pit profiles from the higher accumulation sites (group I) do not fit an exponential function but instead show periodic variability in mass fraction and isotopic composition of NO_3^- (Fig. 3).

As discussed above, sharp decreases in $w(NO_3^-)$ in the top few centimeters of inland East Antarctic snowpits are interpreted as evidence of severe photolytic NO_3^- loss. $w(NO_3^-)$ in the top 10 cm of the coastal P1 snowpit also decreases from the surface (Fig. 3) and, if viewed in isolation, could also be taken as evidence for post-depositional loss. However, annual average snow accumulation at P1 is approximately 50 cm snow a^{-1}, and the full profile clearly shows that similarly high $w(NO_3^-)$ values are observed below 10 cm, as would be expected from seasonal cycles. We expect that if the coastal sites studied by Erbland et al. (2013) had been continuously sampled below 20 cm, similar features would have been observed. This should serve as caution in interpreting the behavior of NO_3^- at high accumulation sites based on observations that do not cover a full annual cycle of snowfall.

Although a significant correlation between $\ln(1+\delta^{15}N)$ and $\ln(w(NO_3^-))$ was observed in the upper snow layers (upper 20, 40 and 60 cm; Table 2) in P3, no relationship was found between the two parameters when the top most sample was removed ($\ln(1+\delta^{15}N)$ vs. $\ln(w(NO_3^-))$ in P3; Fig. 5). This is different from the inland snowpits, where the top most sample is less influential on the linear fit (i.e., $\ln(1+\delta^{15}N)$ vs. $\ln(w(NO_3^-))$ in P4–P7; Fig. 5). In addition, the $^{15}\varepsilon_{app}$ values found in P3, while statistically significant, are much higher than those calculated for P4–P7 (Table 2). The $^{18}\varepsilon_{app}$ is almost entirely not statistically significant for P1, P2 and P3. In the case of the group I snowpits, the relationships amongst $\delta^{15}N(NO_3^-)$, $\delta^{18}O(NO_3^-)$, and $w(NO_3^-)$ are difficult to interpret as evidence of photolysis (Figs. 4 and 5).

Profiles of the group I pits (P1–P3) show large variations in $w(NO_3^-)$ and isotopic composition throughout the snowpack, with some correspondence to $\delta^{18}O(H_2O)$ which is a proxy for temperature (Fig. 7; see also Fig. 3). The seasonality is most apparent at site P1 due to the highest sampling resolution (3.0 cm per sample compared to 5.0 cm per sample for pits P2 and P3) and highest snow accumulation rate (172 kg m^{-2} a^{-1}), though all group I sites feature high accumulation rates above 91 kg m^{-2} a^{-1} (Table 1).

It is difficult to assign samples to four distinct seasons based on $\delta^{18}O(H_2O)$ alone, so we choose a conservative classification of two periods: a warm season corresponding to higher $\delta^{18}O(H_2O)$ and a cold season characterized by lower $\delta^{18}O(H_2O)$ (Fig. 7). These assignments are also consistent with other established seasonal tracers measured in P1 in that the $\delta^{18}O(H_2O)$ peaks (warm season) correspond to spikes in methanesulfonic acid and low Na^+ mass fractions, while the opposite pattern is present during the identified cold seasons (C.-J. Li, personal communication, 2014). The snow ac-

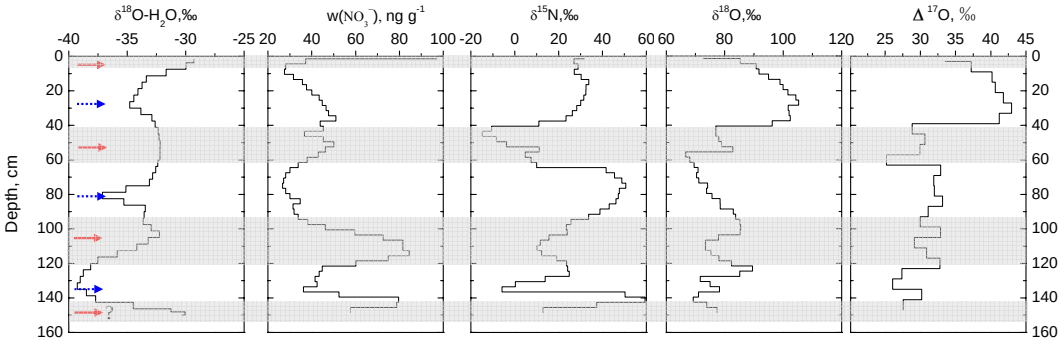

Figure 7. Seasonality in $w(NO_3^-)$, $\delta^{15}N$, $\delta^{18}O$ and $\Delta^{17}O$ of NO_3^- in the P1 snowpit. Red solid arrows and blue dashed arrows represent the middle of the identified warm and cold seasons, respectively, and shaded areas denote warm seasons (see text). One seasonal cycle represents one $\delta^{18}O(H_2O)$ peak to the next. Seasonal assignment of snow near the pit base is subject to uncertainty due to the limited coverage and absent comparison with a preceding cold season.

cumulation rate of 172 kg m^{-2} a^{-1} at P1 site, which corresponds to 43–57 cm snow a^{-1} assuming a typical snow density of 0.3–0.4 g cm^{-3}, also fits with the thickness of the designated seasonal layers. Although coarse, this conservative dating of the snowpit is sufficient to make broad comparisons throughout the year. This is aided by the high accumulation rate and the large amplitude variability in the data.

The samples and data assigned to warm and cold seasons for P1 are shown in Figs. 7 and 8. If the $\delta^{18}O(H_2O)$ peaks are taken to roughly correspond with the middle of the warm season, this results in 62 % of samples falling into the cold season compared with the warm season, which agrees well with the seasonal precipitation climatology where conditions slightly favor cold season accumulation (e.g., about 60 % of snow occurs in the cold season on the coast; Laepple et al., 2011).

As illustrated in Fig. 7, snow $w(NO_3^-)$ spikes are present during the warm periods, while $w(NO_3^-)$ in the cold season is lower. The averages of $w(NO_3^-)$ in warm and cold seasons are 62.0 and 36.6 ng g^{-1}, respectively (Fig. 8a). Previous observations at Antarctic coastal sites suggested that NO_3^- mass fractions were generally higher in summer and lower in winter (Mulvaney et al., 1998; Wagenbach et al., 1998; Wolff et al., 2008), which is consistent with our findings. In contrast, values of $\delta^{15}N$, $\delta^{18}O$ and $\Delta^{17}O$ of NO_3^-, are all higher in cold seasons (with means of 31.0, 86.3 and 34.4 ‰, respectively); while the averages in warm seasons are 12.6, 77.4 and 30.4 ‰, respectively (Fig. 8a).

Photolytic loss of NO_3^- at high accumulation sites such as Summit, Greenland (where the 200 kg m^{-2} a^{-1} accumulation rate is comparable to P1) appears to be negligible (Hastings et al., 2004; Fibiger et al., 2013). In addition, the expected negative relationship between $w(NO_3^-)$ and $\delta^{15}N(NO_3^-)$ based upon the negative photolytic $^{15}\varepsilon$ (−45.3 ‰) is not observed nor does $\delta^{15}N(NO_3^-)$ show a sharp increase with the decreasing $w(NO_3^-)$ in the upper 10 cm. Furthermore, given the results from the inland pits, a higher degree of photolytic NO_3^- loss (i.e., the extent of photolysis) could be expected to be accompanied by more secondary oxidation in the condensed phase (e.g., Jacobi and Hilker, 2007), leading to a decrease of $\delta^{18}O(NO_3^-)$ in the upper snowpack. But there is a significant increasing trend of $\delta^{18}O(NO_3^-)$ in the upper 30 cm of snow (Fig. 7), and there is no relationship between $\delta^{15}N(NO_3^-)$ and $\delta^{18}O(NO_3^-)$ in the data set as a whole or when divided by season. Thus, it is concluded that photolytic loss of NO_3^- at P1 is likely not influential.

If volatilization was driving the variability of $w(NO_3^-)$, a relationship between $w(NO_3^-)$ and $\delta^{15}N(NO_3^-)$ could be expected based on the theoretically calculated value for $^{15}\varepsilon$ (Table S3 in the Supplement), but none is observed (Table 2). On the other hand, the $^{15}\varepsilon$ value at −20 °C reported from the Dome C experiment ($^{15}\varepsilon = -0.3$ ‰) is effectively non-fractionating (Erbland et al., 2013). Based on this, it is difficult to attribute the isotopic variability in P1 to volatilization.

In summary, the observed variability in $w(NO_3^-)$ and isotopic composition cannot be explained by post-depositional processes in snow, given our current knowledge of isotopic fractionations by the processes discussed above. The observed large variations in the P1 isotopic and mass fraction data are more plausibly explained as presenting a seasonal NO_3^- source shift over different periods (see below), which may be further corroborated by the changing relationship of $w(NO_3^-)$ vs. $\delta^{18}O(NO_3^-)$ between cold and warm seasons (Fig. 8b).

A number of studies have suggested that the stratosphere is the primary source of NO_3^- to the Antarctic ice sheet (Mulvaney and Wolff, 1993; Wagenbach et al., 1998; Savarino et al., 2007), with an estimated annual flux of $6.3 \pm 2.7 \times 10^7$ kg N a^{-1} (Muscari et al., 2003). As discussed by Savarino et al. (2007), interactions between NO_x and stratospheric ozone lead to some of the highest $\Delta^{17}O$ (and $\delta^{18}O$) of NO_3^- values, which have thus far only been observed in polar regions. It is notable that $\delta^{18}O(NO_3^-)$ val-

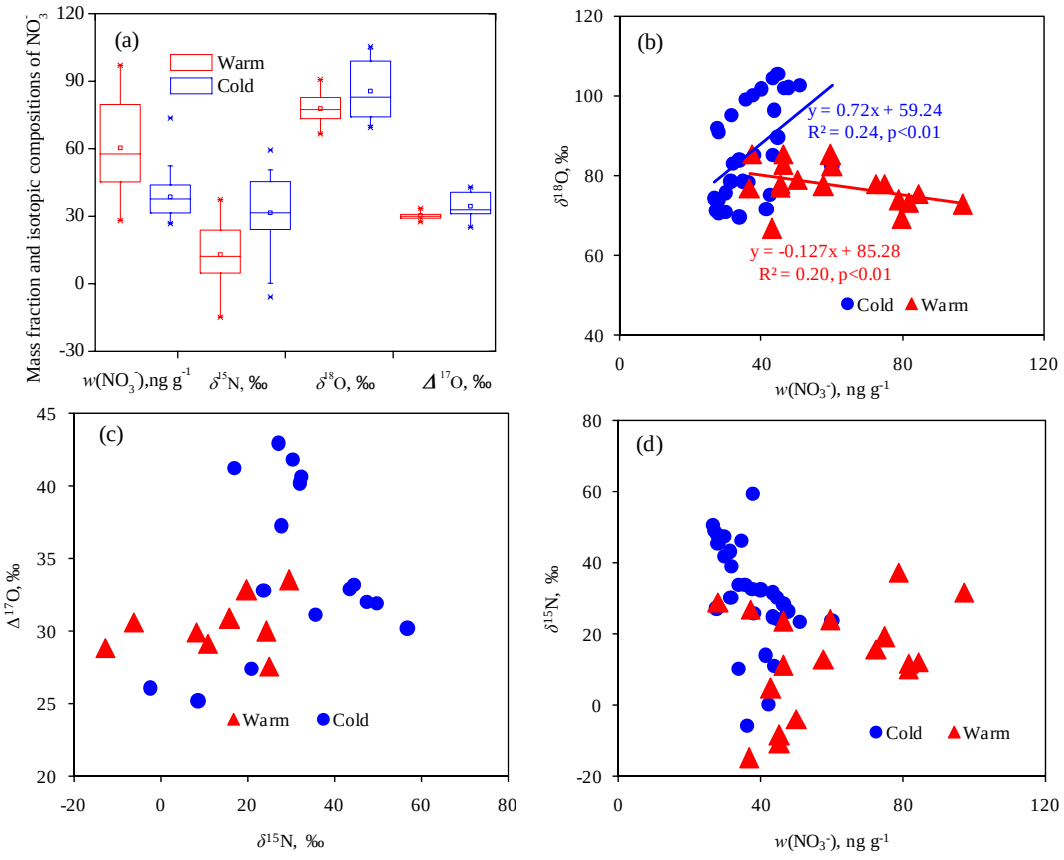

Figure 8. $w(NO_3^-)$, $\delta^{15}N$, $\delta^{18}O$ and $\Delta^{17}O$ of NO_3^- in warm and cold season samples from snowpit P1. Summary statistics by season are shown in **(a)**, with box and whisker plots representing maximum (top X symbol), minimum (bottom X symbol), percentiles (5th, 25th, 75th, and 95th), and median (50th, solid line) and mean (open square near center of each box). The seasonal relationships between $w(NO_3^-)$ and $\delta^{18}O$, $\delta^{15}N$ and $\Delta^{17}O$, and $w(NO_3^-)$ and $\delta^{15}N$ of NO_3^- are shown in **(b)**, **(c)** and **(d)** respectively.

ues above 90 ‰ are all present in cold season snow (Fig. 7), and $\delta^{18}O(NO_3^-)$ and $\Delta^{17}O(NO_3^-)$ (ranging from 69.5 to 105.3 ‰ and 25.2 to 42.9 ‰, respectively) in this period are comparable to the data of atmospheric NO_3^- (inorganic NO_3^- aerosol) in winter at the coastal East Antarctic Dumont d'Urville station (DDU; 66°40′ S, l40°01′ E). At DDU, the higher $\delta^{18}O(NO_3^-)$ and $\Delta^{17}O(NO_3^-)$ in winter is thought to be linked with stratospheric NO_3^- deposition (Savarino et al., 2007). The great enrichment of ^{18}O and ^{17}O in the cold season NO_3^- in P1 suggests that O atoms from stratospheric O_3 have been incorporated into NO_x and NO_3^- (Reactions R4–R6) that was subsequently deposited in snow as NO_3^-. However, whether this influence of stratospheric O_3 occurs in the stratosphere or troposphere is not distinguishable.

Interestingly, the highest $\delta^{18}O(NO_3^-)$ and $\Delta^{17}O(NO_3^-)$ values are all found in the most recent winter/spring in P1, namely 2012. This season was marked by much less stratospheric O_3 loss and a smaller O_3 hole extent than in previous seasons covered by the P1 snowpit; the mean 2012 O_3 hole area was 19 % smaller than the prior 3-year average, and the minimum O_3 concentration of 139.1 DU detected by satellite was the highest on record since 1988 (based on data from the NASA Goddard Space Flight Center: http://ozonewatch.gsfc.nasa.gov/meteorology/annual_data.txt). This might support that, where atmospheric NO_3^- is preserved in Antarctic snow, the O isotopes of NO_3^- could track stratospheric O_3 changes over time (McCabe et al., 2007).

At the South Pole, McCabe et al. (2007) suggested that the $\Delta^{17}O(NO_3^-)$ may track changes in stratospheric ozone. However, McCabe et al. (2007) found an anti-correlation between $\Delta^{17}O(NO_3^-)$ with October–December column ozone concentrations. Two hypotheses were proposed in this work: (1) the NO_3^- oxygen isotopes are being primarily affected by increases in tropospheric ozone levels because of increased UV from decreased springtime column ozone levels, or (2) the oxygen isotopes are recording increases in the stratospheric NO_3^- flux during years of reduced column ozone. At the South Pole, NO_3^- in snow is expected to preserve only 25 % of the original stratospheric isotopic composition, whereas 75 % reflects the tropospheric isotopic composition, due to NO_3^- produced locally from the snow-sourced, gas-phase re-

cycled NO_x on the polar plateau (McCabe et al., 2007). The situation is quite different at coastal site P1, where the photolysis imprint is rather minor. For snow NO_3^- in the cold season at P1, higher $\delta^{18}O(NO_3^-)$ and $\Delta^{17}O(NO_3^-)$ correspond to a smaller ozone hole (i.e., column ozone is higher), and this is most dramatic in 2012.

The $\delta^{15}N(NO_3^-)$ in P1 cold season snow has a mean of 31.0 ± 14.5 ‰, which is much higher than that found in atmospheric NO_3^- at DDU (maximum of 10.8 ‰). Further, the highest values of $\delta^{15}N(NO_3^-)$ are only observed in cold season snow, in more than 1 year (Figs. 7 and 8). Savarino et al. (2007) calculated that the isotopic signature of NO formed in the stratosphere would be 19 ± 3 ‰ based upon the estimated fractionation of N_2O upon decomposition. Based on the expectation that more than 90 % of stratospheric NO_y (sum of reactive nitrogen oxide compounds) is removed during denitrification, Savarino et al. (2007) further predicted that the $\delta^{15}N$ of NO is close to the $\delta^{15}N(NO_3^-)$. But values of 19 ‰ are much greater than that found by Moore (1974), who collected NO_3^- via balloons raised to 21–27 km and determined $\delta^{15}N(NO_3^-)$ values of 0.8–2.8 ‰ ($n = 7$) over Alaska and Australia. The much higher values found in coastal snow must then represent either a higher stratospheric $\delta^{15}N$ source value than predicted, or fractionation associated with chemistry, transport or deposition. The annual weighted average $\delta^{15}N(NO_3^-)$ in a skin layer of snow at the air–snow interface was found to be 24.7 ‰ higher than that in atmospheric NO_3^- and it was suggested that this was due to a fractionation associated with deposition (Erbland et al., 2013). A striking difference between $\delta^{18}O(NO_3^-)$ and $\Delta^{17}O(NO_3^-)$ in atmospheric NO_3^- and that in the skin layer was not found, and instead the oxygen isotopes were suggested to be in equilibrium. The $\delta^{18}O(NO_3^-)$ in P1 and the correlation of $\delta^{18}O(NO_3^-)$ and $\Delta^{17}O(NO_3^-)$ ($R^2 = 0.77$, $p < 0.01$) fit well within the range expected for primary atmospheric NO_3^-, and it is unlikely that significant fractionation associated with deposition (or chemistry or transport) would affect only $\delta^{15}N(NO_3^-)$ and not $\delta^{18}O(NO_3^-)$. It seems possible then that a higher $\delta^{15}N(NO_3^-)$ value (or range) than 19 ‰ from stratospheric denitrification, or an alternative source (see below) is needed to explain the P1 cold season data.

The warm season snow in P1 exhibits lower mean $\delta^{15}N$, $\delta^{18}O$ and $\Delta^{17}O$ of NO_3^- (Fig. 8a). These lower values, and the occurrence of $\delta^{15}N(NO_3^-) < 0$ ‰ in warm seasons, are also consistent with the DDU atmospheric data (Savarino et al., 2007). The very low and negative $\delta^{15}N(NO_3^-)$ values found between October and December at DDU were interpreted as resulting from HNO_3 formed in the atmosphere from snow-sourced NO_x emissions transported from the plateau. Namely, the release of NO_x from photolysis of surface snow NO_3^- can explain these values because of the very large and negative $^{15}\varepsilon$ (see Sect. 4.1.1 above). The seasonally lowered O isotopic composition can then be explained as arising from the gas-phase oxidation of snow-sourced NO_x to HNO_3 predominantly by OH (Reaction R3), which would be expected to be the predominant pathway of HNO_3 formation during the warm season (Alexander et al., 2009).

While the mean values shown in Fig. 8a are representative of the seasonal shifts in the isotopic composition of NO_3^-, it is also clear from Fig. 7 that there is significant interannual variability. A recent adjoint modeling study suggested that $w(NO_3^-)$ in Antarctic snow was most sensitive to tropospheric sources of NO_x, primarily fossil fuel combustion, biogenic soil emissions and lightning, though snow emissions were not considered in the model (Lee et al., 2014). The isotopic signatures of NO_x sources and their relationship with the $\delta^{15}N$ of NO_3^- are poorly constrained (e.g., Fibiger et al., 2014), particularly in the Southern Hemisphere. For example, the $\delta^{15}N$ of NO_x from vehicle emissions in South Africa were consistently negative (Heaton, 1990) while the $\delta^{15}N$ of NO_x from vehicle emissions found in Switzerland was mostly positive (Ammann et al., 1999), and a recent study in the US suggests very positive values associated with vehicle emissions (Felix and Elliott, 2014). Natural, biogenic soil emissions have not been directly quantified, but fertilized soils in a laboratory study emitted NO_x with very low $\delta^{15}N$ (from -48.9 to -19.9 ‰) (Li and Wang, 2008), and lightning-sourced NO_x is expected to be near 0 ‰. Additionally, peroxyacetyl nitrate (PAN) is suggested as an important source of NO_x to the Antarctic atmosphere during the warm season (Lee et al., 2014). While no direct information is available in terms of the $\delta^{15}N$ of NO_x (or NO_3^-) produced from PAN decomposition, it has been suggested that this could explain sporadic high $\delta^{15}N$ of NO_3^- in the northern subtropical marine system (Altieri et al., 2013). It is not possible at this time to link the observed changes in isotopic composition directly to NO_x emission sources. Still, qualitatively, and based on the combination of isotopes, the P1 snowpit data would agree with a varying relative contribution of tropospheric NO_x sources from year-to-year in the warm season. In the cold season, the data suggest that there is still an important degree of stratospheric influence on NO_3^- loading in Antarctic snow, particularly in 2012 when the O_3 hole was unusually small.

5 Conclusions

The purpose of this study was to investigate the effects of post-depositional processes on isotopic fractionation of NO_3^- at different depths in the snowpack, and to understand variation of NO_3^- isotopic composition in different environments on the EAIS. In the EAIS interior, where accumulation rates are very low (group II snowpits; $< 55\,kg\,m^{-2}\,a^{-1}$), a high degree of NO_3^- loss is found. The high values of $\delta^{15}N(NO_3^-)$ found in near-surface snow (i.e., top 20 cm) and the relationship between $w(NO_3^-)$ and $\delta^{15}N(NO_3^-)$ are consistent with a Rayleigh-type process and theoretically pre-

dicted $^{15}\varepsilon$ values for NO_3^- photolysis. The concurrent decreases in $\delta^{18}O(NO_3^-)$, however, are best explained as resulting from condensed-phase re-oxidation forming secondary NO_3^- that contains oxygen atoms derived from in situ H_2O (e.g., $\delta^{18}O(H_2O)$ of −60 ‰). This significantly decreases the $\delta^{18}O(NO_3^-)$ overall from what was originally deposited, and explains the positive relationship between $w(NO_3^-)$ and the $\delta^{18}O$ of NO_3^- (and therefore the positive observed $^{18}\varepsilon_{app}$ values). Interestingly, below 20 cm in the group II snowpits, a change in the relationship between $w(NO_3^-)$ and $\delta^{18}O(NO_3^-)$ is observed. These findings highlight the utility of the combined use of $\delta^{15}N(NO_3^-)$ and $\delta^{18}O(NO_3^-)$ for detecting post-depositional processing of NO_3^- and the difficulty in predicting the isotopic composition of NO_3^- at depth based on the fractionation of near-surface NO_3^- alone. We find that in both group II and group I snowpits (accumulation $> 91\,kg\,m^{-2}\,a^{-1}$), $w(NO_3^-)$, $\delta^{15}N(NO_3^-)$, and $\delta^{18}O(NO_3^-)$ cannot be fit by a simple exponential model, implying that photolytic loss cannot be assumed to operate consistently over time. In the case of the group II snowpits, a significant negative relationship is observed between $w(NO_3^-)$ and $\delta^{18}O(NO_3^-)$ at depths between 100 and 200 cm. We suggest that the change over time in the behavior of the isotopes is best explained as being driven by changes in the photolability of NO_3^- and thus, chemistry of the snow. In the case of the group I snowpits, seasonal variability is found in $w(NO_3^-)$, $\delta^{15}N$, $\delta^{18}O$, and $\Delta^{17}O$ of NO_3^- throughout the profiles. We suggest that the seasonality observed in higher accumulation, more coastal EAIS sites is driven by the influence of seasonal changes in NO_3^- sources. The best explanation for the range of values seen, given current knowledge, is the importance of stratospheric ozone influence on the production of atmospheric NO_3^- in the cold season compared to more tropospheric NO_x source influence in the warm season.

The Supplement related to this article is available online at doi:10.5194/acp-15-9435-2015-supplement.

Acknowledgements. This research was supported by the National Science Foundation of China (Grant nos. 41206188 to GS, 41476169 to SJ), the US National Science Foundation Antarctic Glaciology Program (Grant no. 1246223 to MGH) and Chinese Polar Environment Comprehensive Investigation and Assessment Programmes (Grant nos. CHINARE 2014-02-02 to BS, 2014-04-01 to GS). We are also grateful to Ruby Ho at Brown University and the 29th CHINARE inland members for technical support and assistance, and Dr. Erbland, two anonymous reviewers and the editor for their helpful comments.

Edited by: J. Kaiser

References

Alexander, B., Savarino, J., Kreutz, K. J., and Thiemens, M.: Impact of preindustrial biomass-burning emissions on the oxidation pathways of tropospheric sulfur and nitrogen, J. Geophys. Res., 109, D08303, doi:10.1029/2003JD004218, 2004.

Alexander, B., Hastings, M. G., Allman, D. J., Dachs, J., Thornton, J. A., and Kunasek, S. A.: Quantifying atmospheric nitrate formation pathways based on a global model of the oxygen isotopic composition ($\Delta^{17}O$) of atmospheric nitrate, Atmos. Chem. Phys., 9, 5043–5056, doi:10.5194/acp-9-5043-2009, 2009.

Altieri, K., Hastings, M., Gobel, A., Peters, A., and Sigman, D.: Isotopic composition of rainwater nitrate at Bermuda: The influence of air mass source and chemistry in the marine boundary layer, J. Geophys. Res., 118, 11304–11316, 2013.

Ammann, M., Siegwolf, R., Pichlmayer, F., Suter, M., Saurer, M., and Brunold, C.: Estimating the uptake of traffic-derived NO_2 from ^{15}N abundance in Norway spruce needles, Oecologia, 118, 124–131, 1999.

Böhlke, J., Mroczkowski, S., and Coplen, T.: Oxygen isotopes in nitrate: New reference materials for ^{18}O: ^{17}O: ^{16}O measurements and observations on nitrate-water equilibration, Rapid Commun. Mass. Sp., 17, 1835–1846, 2003.

Berhanu, T. A., Meusinger, C., Erbland, J., Jost, R., Bhattacharya, S., Johnson, M. S., and Savarino, J.: Laboratory study of nitrate photolysis in Antarctic snow. II. Isotopic effects and wavelength dependence, J. Chem. Phy., 140, 244306, doi:10.1063/1.4882899, 2014.

Blunier, T., Floch, G., Jacobi, H.-W., and Quansah, E.: Isotopic view on nitrate loss in Antarctic surface snow, Geophys. Res. Lett., 32, L13501, doi:10.1029/2005GL023011, 2005.

Boxe, C., Colussi, A., Hoffmann, M., Murphy, J., Wooldridge, P., Bertram, T., and Cohen, R.: Photochemical production and release of gaseous NO_2 from nitrate-doped water ice, J. Phys. Chem., 109, 8520–8525, 2005.

Buffen, A. M., Hastings, M. G., Thompson, L. G., and Mosley-Thompson, E.: Investigating the preservation of nitrate isotopic composition in a tropical ice core from the Quelccaya Ice Cap, Peru, J. Geophys. Res., 119, 2674–2697, doi:10.1002/2013JD020715, 2014.

Bunton, C., Halevi, E., and Llewellyn, D.: Oxygen exchange between nitric acid and water. Part I, J. Chem. Soc., 4913–4916, doi:10.1039/jr9520004913, 1952.

Casciotti, K., Sigman, D., Hastings, M. G., Böhlke, J., and Hilkert, A.: Measurement of the oxygen isotopic composition of nitrate in seawater and freshwater using the denitrifier method, Anal. Chem., 74, 4905–4912, 2002.

Chu, L. and Anastasio, C.: Quantum yields of hydroxyl radical and nitrogen dioxide from the photolysis of nitrate on ice, J. Phys. Chem., 107, 9594–9602, 2003.

Criss, R. E.: Principles of stable isotope distribution, Oxford University Press, New York, 254 pp., 1999.

Davis, D. D., Seelig, J., Huey, G., Crawford, J., Chen, G., Wang, Y., Buhr, M., Helmig, D., Neff, W., Blake, D., Arimot, R., and Eisele, F.: A reassessment of Antarctic plateau reactive nitrogen based on ANTCI 2003 airborne and ground based measurements, Atmos. Environ., 42, 2831–2848, 2008.

Delmas, R., Serca, D., and Jambert, C.: Global inventory of NO_x sources, Nutr. Cycl. Agroecosys, 48, 51–60, 1997.

Dibb, J. E. and Fahnestock, M.: Snow accumulation, surface height change, and firn densification at Summit, Greenland: Insights from 2 years of in situ observation, J. Geophys. Res., 109, D24113, doi:10.1029/2003JD004300, 2004.

Dibb, J. E., Arsenault, M., Peterson, M. C., and Honrath, R. E.: Fast nitrogen oxide photochemistry in Summit, Greenland snow, Atmos. Environ., 36, 2501–2511, 2002.

Ding, M., Xiao, C., Jin, B., Ren, J., Qin, D., and Sun, W.: Distribution of δ^{18}O in surface snow along a transect from Zhongshan Station to Dome A, East Antarctica, Chin. Sci. Bull., 55, 2709–2714, 2010.

Ding, M., Xiao, C., Li, Y., Ren, J., Hou, S., Jin, B., and Sun, B.: Spatial variability of surface mass balance along a traverse route from Zhongshan station to Dome A, Antarctica, J. Glaciol., 57, 658–666, 2011.

Dubowski, Y., Colussi, A., and Hoffmann, M.: Nitrogen dioxide release in the 302 nm band photolysis of spray-frozen aqueous nitrate solutions. Atmospheric implications, J. Phys. Chem., 105, 4928–4932, 2001.

Elliott, E. M., Kendall, C., Wankel, S. D., Burns, D. A., Boyer, E. W., Harlin, K., Bain, D. J., and Butler, T. J.: Nitrogen isotopes as indicators of NO_x source contributions to atmospheric nitrate deposition across the midwestern and northeastern United States, Environ. Sci. Technol., 41, 7661–7667, doi:10.1021/es070898t, 2007.

Erbland, J., Vicars, W. C., Savarino, J., Morin, S., Frey, M. M., Frosini, D., Vince, E., and Martins, J. M. F.: Air–snow transfer of nitrate on the East Antarctic Plateau – Part 1: Isotopic evidence for a photolytically driven dynamic equilibrium in summer, Atmos. Chem. Phys., 13, 6403–6419, doi:10.5194/acp-13-6403-2013, 2013.

Felix, J. D. and Elliott, E. M.: Isotopic composition of passively collected nitrogen dioxide emissions: Vehicle, soil and livestock source signatures, Atmos. Environ., 92, 359–366, 2014.

Fibiger, D. L.: Investigating post-depositional processing of nitrate in snow and constraining NO_x emissions sources using the isotopes of nitrate, PhD, Geological Sciences, Brown University, Providence, 105 pp., 2014.

Fibiger, D. L., Hastings, M. G., Dibb, J. E., and Huey, L. G.: The preservation of atmospheric nitrate in snow at Summit, Greenland, Geophys. Res. Lett., 40, 3484–3489, 2013.

Frey, M. M., Savarino, J., Morin, S., Erbland, J., and Martins, J. M. F.: Photolysis imprint in the nitrate stable isotope signal in snow and atmosphere of East Antarctica and implications for reactive nitrogen cycling, Atmos. Chem. Phys., 9, 8681–8696, doi:10.5194/acp-9-8681-2009, 2009.

Grannas, A. M., Jones, A. E., Dibb, J., Ammann, M., Anastasio, C., Beine, H. J., Bergin, M., Bottenheim, J., Boxe, C. S., Carver, G., Chen, G., Crawford, J. H., Dominé, F., Frey, M. M., Guzmán, M. I., Heard, D. E., Helmig, D., Hoffmann, M. R., Honrath, R. E., Huey, L. G., Hutterli, M., Jacobi, H. W., Klán, P., Lefer, B., McConnell, J., Plane, J., Sander, R., Savarino, J., Shepson, P. B., Simpson, W. R., Sodeau, J. R., von Glasow, R., Weller, R., Wolff, E. W., and Zhu, T.: An overview of snow photochemistry: evidence, mechanisms and impacts, Atmos. Chem. Phys., 7, 4329–4373, doi:10.5194/acp-7-4329-2007, 2007.

Hastings, M. G.: Evaluating source, chemistry and climate change based upon the isotopic composition of nitrate in ice cores, IOP C. Ser. Earth Env., 9, 012002, doi:10.1088/1755-1315/9/1/012002, 2010.

Hastings, M. G., Sigman, D. M., and Lipschultz, F.: Isotopic evidence for source changes of nitrate in rain at Bermuda, J. Geophys. Res., 108, 4790, doi:10.1029/2003JD003789, 2003.

Hastings, M. G., Steig, E., and Sigman, D.: Seasonal variations in N and O isotopes of nitrate in snow at Summit, Greenland: Implications for the study of nitrate in snow and ice cores, J. Geophys. Res., 109, D20306, doi:10.1029/2004JD004991, 2004.

Hastings, M. G., Jarvis, J. C., and Steig, E. J.: Anthropogenic impacts on nitrogen isotopes of ice-core nitrate, Science, 324, 1288–1288, 2009.

Heaton, T. H. E.: $^{15}N/^{14}N$ ratios of NO_x from vehicle engines and coal-fired power stations, Tellus B, 42, 304–307, 1990.

Jacobi, H.-W. and Hilker, B.: A mechanism for the photochemical transformation of nitrate in snow, J. Photoch. Photobio. A, 185, 371–382, 2007.

Johnsen, S. J., Clausen, H. B., Dansgaard, W., Gundestrup, N. S., Hammer, C. U., Andersen, U., Andersen, K. K., Hvidberg, C. S., Dahl-Jensen, D., and Steffensen, J. P.: The δ^{18}O record along the Greenland Ice Core Project deep ice core and the problem of possible Eemian climatic instability, J. Geophys. Res., 102, 26397–26410, 1997.

Kaiser, J., Hastings, M. G., Houlton, B. Z., Röckmann, T., and Sigman, D. M.: Triple oxygen isotope analysis of nitrate using the denitrifier method and thermal decomposition of N_2O, Anal. Chem., 79, 599–607, 2007.

Laepple, T., Werner, M., and Lohmann, G.: Synchronicity of Antarctic temperatures and local solar insolation on orbital timescales, Nature, 471, 91–94, 2011.

Lee, D., Köhler, I., Grobler, E., Rohrer, F., Sausen, R., Gallardo-Klenner, L., Olivier, J., Dentener, F., and Bouwman, A.: Estimations of global NO_x, emissions and their uncertainties, Atmos. Environ., 31, 1735–1749, 1997.

Lee, H.-M., Henze, D. K., Alexander, B., and Murray, L. T.: Investigating the sensitivity of surface-level nitrate seasonality in Antarctica to primary sources using a global model, Atmos. Environ., 89, 757–767, 2014.

Li, D. and Wang, X.: Nitrogen isotopic signature of soil-released nitric oxide (NO) after fertilizer application, Atmos. Environ., 42, 4747–4754, 2008.

Madronich, S. and Flocke, S.: The role of solar radiation in atmospheric chemistry, in: Handbook of Environmental Chemistry, edited by: Boule, P., Springer Verlag, Heidelberg, 1–26, 1998.

Mayewski, P. A. and Legrand, M. R.: Recent increase in nitrate concentration of Antarctic snow, Nature, 346, 258–260, 1990.

McCabe, J., Boxe, C., Colussi, A., Hoffmann, M., and Thiemens, M.: Oxygen isotopic fractionation in the photochemistry of nitrate in water and ice, J. Geophys. Res., 110, D15310, doi:10.1029/2004JD005484, 2005.

McCabe, J. R., Thiemens, M. H., and Savarino, J.: A record of ozone variability in South Pole Antarctic snow: Role of nitrate oxygen isotopes, J. Geophys. Res., 112, D12303, doi:10.1029/2006JD007822, 2007.

Meusinger, C., Berhanu, T. A., Erbland, J., Savarino, J., and Johnson, M. S.: Laboratory study of nitrate photolysis in Antarctic snow. I. Observed quantum yield, domain of photolysis, and secondary chemistry, J. Chem. Phys., 140, 244305, doi:10.1063/1.4882898, 2014.

Michalski, G., Savarino, J., Böhlke, J., and Thiemens, M.: Determination of the total oxygen isotopic composition of nitrate and the calibration of a $\Delta^{17}O$ nitrate reference material, Anal. Chem., 74, 4989–4993, 2002.

Michalski, G., Scott, Z., Kabiling, M., and Thiemens, M. H.: First measurements and modeling of $\Delta^{17}O$ in atmospheric nitrate, Geophys. Res. Lett., 30, 1870, doi:10.1029/2003GL017015, 2003.

Moore, H.: Isotopic measurement of atmospheric nitrogen compounds, Tellus, 26, 169–174, 1974.

Morin, S., Savarino, J., Frey, M. M., Yan, N., Bekki, S., Bottenheim, J. W., and Martins, J. M.: Tracing the origin and fate of NO_x in the Arctic atmosphere using stable isotopes in nitrate, Science, 322, 730–732, 2008.

Mulvaney, R. and Wolff, E.: Evidence for winter/spring denitrification of the stratosphere in the nitrate record of Antarctic firn cores, J. Geophys. Res., 98, 5213–5220, 1993.

Mulvaney, R., Wagenbach, D., and Wolff, E. W.: Postdepositional change in snowpack nitrate from observation of year-round near-surface snow in coastal Antarctica, J. Geophys. Res., 103, 11021–11031, 1998.

Muscari, G., de Zafra, R. L., and Smyshlyaev, S.: Evolution of the NO_y-N_2O correlation in the Antarctic stratosphere during 1993 and 1995, J. Geophys. Res., 108, 4428, doi:10.1029/2002JD002871, 2003.

Röthlisberger, R., Hutterli, M. A., Sommer, S., Wolff, E. W., and Mulvaney, R.: Factors controlling nitrate in ice cores: Evidence from the Dome C deep ice core, J. Geophys. Res., 105, 20565–20572, 2000.

Röthlisberger, R., Hutterli, M. A., Wolff, E. W., Mulvaney, R., Fischer, H., Bigler, M., Goto-Azuma, K., Hansson, M. E., Ruth, U., and Siggaard-Andersen, M.-L.: Nitrate in Greenland and Antarctic ice cores: A detailed description of post-depositional processes, Ann. Glaciol., 35, 209–216, 2002.

Sato, K., Takenaka, N., Bandow, H., and Maeda, Y.: Evaporation loss of dissolved volatile substances from ice surfaces, J. Phys. Chem., 112, 7600–7607, 2008.

Savarino, J., Kaiser, J., Morin, S., Sigman, D. M., and Thiemens, M. H.: Nitrogen and oxygen isotopic constraints on the origin of atmospheric nitrate in coastal Antarctica, Atmos. Chem. Phys., 7, 1925–1945, doi:10.5194/acp-7-1925-2007, 2007.

Sigman, D. M., Casciotti, K. L., Andreani, M., Barford, C., Galanter, M., and Böhlke, J. K.: A bacterial method for the nitrogen isotopic analysis of nitrate in seawater and freshwater, Anal. Chem., 73, 4145–4153, 2001.

Traversi, R., Becagli, S., Castellano, E., Cerri, O., Morganti, A., Severi, M., and Udisti, R.: Study of Dome C site (East Antartica) variability by comparing chemical stratigraphies, Microchem. J., 92, 7–14, 2009.

Wagenbach, D., Graf, V., Minikin, A., Trefzer, U., Kipfstuhl, J., Oerter, H., and Blindow, N.: Reconnaissance of chemical and isotopic firn properties on top of Berkner Island, Antarctica, Ann. Glaciol., 20, 307–312, 1994.

Wagenbach, D., Legrand, M., Fischer, H., Pichlmayer, F., and Wolff, E. W.: Atmospheric near-surface nitrate at coastal Antarctic sites, J. Geophys. Res., 103, 11007–11020, 1998.

Wang, Y., Sodemann, H., Hou, S., Masson-Delmotte, V., Jouzel, J., and Pang, H.: Snow accumulation and its moisture origin over Dome Argus, Antarctica, Clim. Dynam., 40, 731–742, doi:10.1007/s00382-012-1398-9, 2013.

Warneck, P. and Wurzinger, C.: Product quantum yields for the 305-nm photodecomposition of nitrate in aqueous solution, J. Phys. Chem., 92, 6278–6283, 1988.

Warren, S. G., Brandt, R. E., and Grenfell, T. C.: Visible and near-ultraviolet absorption spectrum of ice from transmission of solar radiation into snow, Appl. Optics, 45, 5320–5334, 2006.

Wolff, E. W.: Nitrate in polar ice, in: in Ice core studies of global biogeochemical cycles, edited by: Delmas, R. J., Springer, New York, 195–224, 1995.

Wolff, E. W., Jones, A. E., Bauguitte, S. J.-B., and Salmon, R. A.: The interpretation of spikes and trends in concentration of nitrate in polar ice cores, based on evidence from snow and atmospheric measurements, Atmos. Chem. Phys., 8, 5627–5634, doi:10.5194/acp-8-5627-2008, 2008.

Wolff, E. W., Bigler, M., Curran, M., Dibb, J., Frey, M., Legrand, M., and McConnell, J.: The Carrington event not observed in most ice core nitrate records, Geophys. Res. Lett., 39, L08503, doi:10.1029/2012GL051603, 2012.

Xiao, C., Ding, M., Masson-Delmotte, V., Zhang, R., Jin, B., Ren, J., Li, C., Werner, M., Wang, Y., and Cui, X.: Stable isotopes in surface snow along a traverse route from Zhongshan station to Dome A, East Antarctica, Clim. Dynam., 41, 2427–2438, 2013.

Yung, Y. L. and Miller, C. E.: Isotopic fractionation of stratospheric nitrous oxide, Science, 278, 1778–1780, doi:10.1126/science.278.5344.1778, 1997.

Zatko, M. C., Grenfell, T. C., Alexander, B., Doherty, S. J., Thomas, J. L., and Yang, X.: The influence of snow grain size and impurities on the vertical profiles of actinic flux and associated NO_x emissions on the Antarctic and Greenland ice sheets, Atmos. Chem. Phys., 13, 3547–3567, doi:10.5194/acp-13-3547-2013, 2013.